Spring 5-10-2018

An Integrative Approach to Evaluating Radiocesium Contamination in Fukushima Prefecture

James Thornhill

An Integrative Approach to Evaluating Radiocesium Contamination in Fukushima Prefecture

Master's Thesis: James Andrew Thornhill

Department of Ecology of Evolution and Organismal Biology

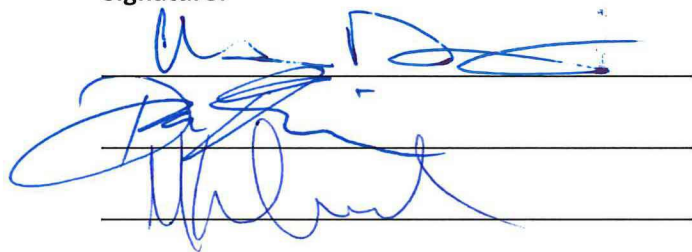Major Professor: Daniel Ferreira, PhD

Date: 10 May 2018

Thesis Approval

Committee Member Name: Signature:

(1) Chris Dockery, PhD

(2) Daniel Ferreira, PhD

(3) Matthew Weand, PhD

Contents

3

Abstract

An earthquake in Japan led to the meltdown of the Fukushima Daiichi Nuclear Power Plant which released radionuclides into the surrounding regions. Of these radionuclides, cesium-137 (^{137}Cs) has been shown to be the most abundant. Research has shown that adsorption of K^+ and Cs^+ on 2:1 clay minerals can collapse the interlayers, causing the adsorbed ion to become non-exchangeable. This study explored these interactions by developing a Cs^+ adsorption envelope on vermiculite and presenting the reaction kinetics of K^+ and Cs^+ to vermiculite adsorption sites. The adsorption envelope results show that, when in the presence of Cs^+, high concentrations of H^+ are needed to compete, even slightly, for adsorption sites. The kinetics experiment did not show K^+ becoming irreversibly bound to vermiculite adsorption sites. The ability of Cs^+ to infiltrate interlayers thought to be collapsed from long-term K^+ exposure provides evidence for Cs^+ being preferentially adsorbed over competing ions. The ecological health and movement of radiocesium in Fukushima Prefecture was monitored using the bioindicators species' bracken ferns and may lilies. Believed to have the capacity for Cs uptake through K channels and carriers, these plant species were observed for physiological changes over a six-month growth period. It could not be concluded that physiological changes observed in the plants were correlated with radiocesium exposure. The plants species have been harvested and are currently undergoing gamma spectrometer analysis for total radiocesium measurement to evaluate their candidacy for phytoremediation trials. A chemical extraction method using ion exchange with Mg^{2+} and a Cs^+-capturing ligand was further developed to elucidate the possibility of radiocesium removal in contaminated soils collected from Fukushima Prefecture. Isolating the clay fraction and removing organic material was necessary to prevent interference with the effectiveness of the Cs^+-capturing ligand and Mg^{2+} ions. Results from this chemical extraction indicate that radiocesium can be removed more efficiently when the clay fraction is properly extracted and isolated from Fukushima Prefecture soils.

Introduction

Fukushima Prefecture is in the Tōhoku region of Japan, approximately north 240 km of Tokyo. It is

divided into coastal and mountain ranges. The coastal regions lie on the Pacific Ocean with the

mountain ranges being further divided into two regions called Aizu and Nakadōri.

Fukushima Daiichi Nuclear Power Plant

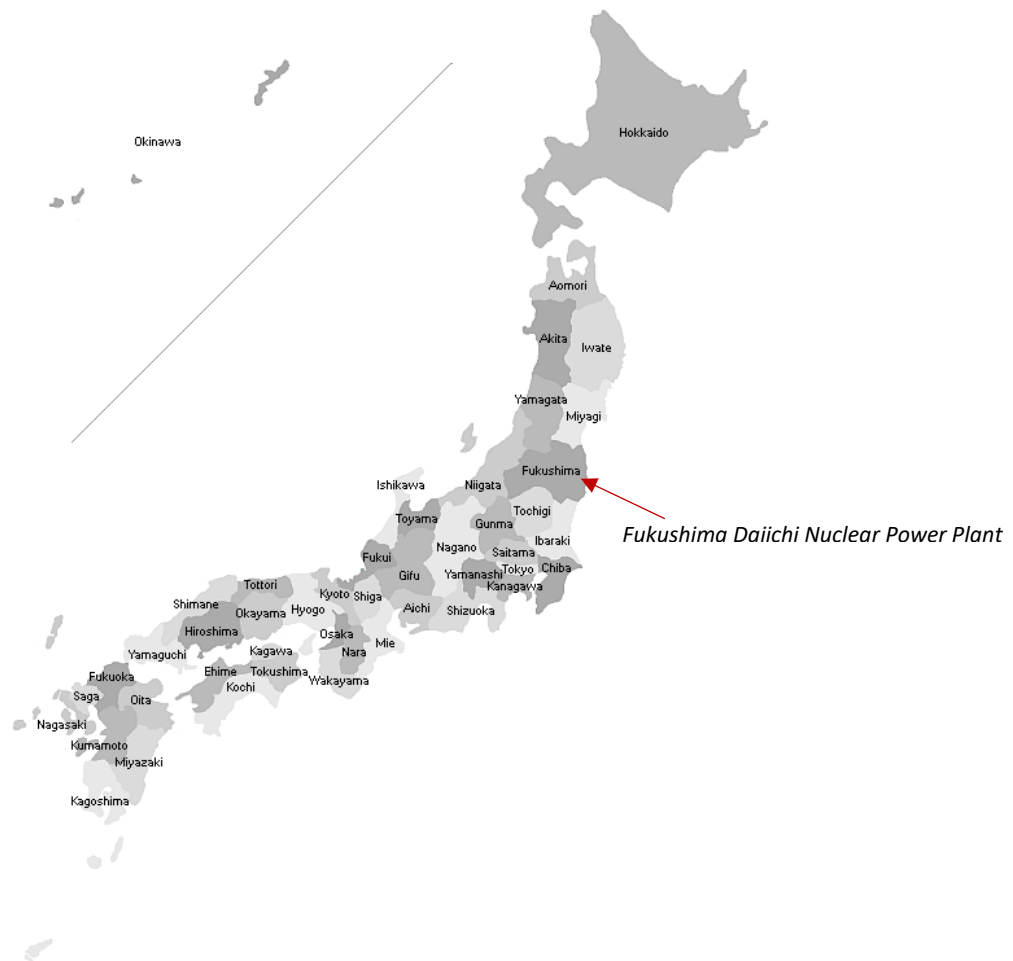**Fig. 1** - Map of Japanese prefectures. Arrow points at Fukushima Daiichi Nuclear Power Plant. Areas

directly around the facility and northwest were impacted by radionuclide release.

https://www.japan-guide.com/list/gif/1002_01.gif

On 11 March 2011, Japan experienced the largest recorded earthquake in its history. The

earthquake, known as the Great East Japan Earthquake, produced a 50-foot tsunami that impacted the

Fukushima Daiichi Nuclear Power Plant (FDNPP) leading to a nuclear meltdown in three of its five reactor units. Due to an inability to keep reactors cool, hydrogen began building up inside the containment structure, causing an explosion that would release a radioactive plume of artificial radionuclides into the surrounding areas of Fukushima Prefecture. Of the radionuclides released at the FDNPP, radiocesium ($^{137}Cs^+$) remains radioactive due to a relatively long half-life (30.2 years). $^{137}Cs^+$ decays primarily by beta emission to the unstable isotope, barium-137m. Barium-137m then decays by the emission of gamma rays to its natural form, barium-137. Gamma rays have the ability of cellular penetration and genetic damage, causing diffuse damage throughout the body and cellular structure (Ward, 2014). Artificial radionuclide contaminated soils are required to cycle through ten half-lives (302 years in the case of $^{137}Cs^+$) before radiation exposure is considered negligible (Mukai 2016). The neighboring lands of FDNPP have been measured with radionuclide depositions of up to 10,000 MBq km^{-2} (Yasunari *et al*. 2011). Investigations have shown that cesium ions remain in the top 5 cm of the soils and that they become strongly fixed as cations on the exchange complex of silty clays (Kagan *et al.* 1996; Kato *et al.* 2012). Soil profiles taken throughout Fukushima Prefecture have concluded that the dominant clay in Fukushima Prefecture is vermiculite (Sano *et al.* 2010; Qin *et al.* 2012; Mukai *et al*. 2016). This strong cationic fixation to vermiculite has created relatively immobile radioactively contaminated soil that persists to be a problem for humans, wildlife, and vegetation (Kamada *et al.* 2012).

The decontamination guidelines released in December 2011 by the Japanese Ministry of the Environment provided detailed the methods for measuring the degree of radioactive contamination in highly affected areas as well as the methods for collection, transport, and storage of the removed topsoil (Japanese Ministry of the Environment 2011). Legislators chose a dig and haul remediation technique that would remove the top 5 centimeters of soil by machinery to be the most effective, economical, and time sensitive given the nature of displaced citizens and the need to restore vital

farmland. Two problems with this approach must be considered for human and environmental safety: (1) the removed topsoil must be replaced with a viable growing soil for agriculture and (2) the contaminated soil must be safely stored and managed while it cycles through the necessary ten radioactive half-lives. It was decided that the alternative soil replacement would be ground up mountains in Fukushima Prefecture. The economic impacts of this approach are staggering with the amount of material and time required for the recycling of contaminated soil. For all agricultural land, the unit cost per hectare to remove the contaminated soil is estimated to cost as much as 40 million Japanese yen (JPY) (Yasutaka and Naito, 2016) or $365,000. The radioactive topsoil must then be stored in environmentally resistant containers (8000 JPY/container), transported to a decontamination site (3100 JPY/container), categorized and later sent to either a combustible (100,000 JPY/container) or incombustible (30,000 JPY/container) storage facility (Shiga Clean Center Website). Contamination containers sent to the incombustible site are covered with a large tarp to further aid in the prevention of environmental degradation. Although there are quantifiable reductions in the contaminated areas, the decontamination effectiveness is limited, and areas remain radioactively contaminated due to the remediation guidelines only requiring the removal of topsoil within 20 meters of habitable areas and roads. Not included in the studies was the need for labor.

This thesis takes an integrative approach to restoration of radiocesium-contaminated soil in three parts by 1) evaluating the adsorption behavior and mechanisms of Cs^+ in vermiculite, 2) using plants as bioindicators to elucidate long-term radiation exposure and testing the bioindicators as possible sources of phytoremediation, and 3) experimenting with a Cs^+-capturing ligand to develop a chemical extraction method that can be used to restore contaminated soil in Fukushima Prefecture. It is the intent of this thesis to provide information that can be used to advance the scientific community's ability to improve Fukushima Prefecture's soil more quickly.

Part One – Cs Adsorption Behavior to Vermiculite

Background

Soil supports and sustains life. Soil serves six main functions: supporting vegetation, regulating water, recycling carbon and other nutrients, regulating atmospheric gases, acting as a habitat for many organisms, and serving as an engineering medium. Soils are the medium by which all people on Earth receive food. Any edible food source at some point is derived from interactions with soil. The loss of such a necessity would be devastating to human life. Unfortunately, the nuclear accident in Fukushima Prefecture caused the loss of many of these functions. With limited land, especially agricultural land, available in Japan, it is of utmost importance that the soils in Fukushima Prefecture be restored to serving all six of these functions.

Properties of Soil

Knowing the properties of soils is vital to remediate $^{137}Cs^+$ from Fukushima Prefecture. The following properties have been well defined for each region of Japan and this information was used to research the Cs^+ binding mechanisms to the soil. The following information provides a means of evaluating the soil in Fukushima Prefecture without prior knowledge of its soil content. The first procedure in determining soil properties is using the feel method. Rubbing soil between two fingers reveals the texture to be smooth, suggesting that Fukushima Prefecture soil has a high clay content. A second property test can be performed using soil that is partially moistened and rolled into a ball. That ball can then be thrown at a vertical surface with its impact yielding aggregate information. Soil aggregates are a group of soil particles that bind to each other more strongly that adjacent particles (USDA Natural Resources Conservation Service, 1996). Fukushima Prefecture soil, with its impact sticking and flattening against the surface, reveals that the soil contains durable aggregates. Clay flocculation, the process by which individual clay particles aggregate into masses, plays a role in the retention of $^{137}Cs^+$ to vermiculite clays in Fukushima Prefecture.   When two negatively charged clay platelets come close together, cations can become compressed between both platelets causing them to be held together.

This led to the confirmation that nuclear reactors near areas with high clay content may not be the best location given the potential for accidents.

Effects of pH

The effects of pH are an important influence on pollutant behavior in clay soils. A study by Rani *et al*. (2012) found that the adsorption capacity of clay is greatly affected by the pH of a solution. They suggest that since the surfaces of clay contain hydroxide (OH^-) groups, a higher pH results in an increase in overall negative charge of the clay surface, increasing the adsorption of cations to the surface. Conversely, as pH decreases, the competition for exchangeable sites begins to be affected by H^+ ions leading to a decrease in cation adsorption. The process of cation adsorption and ion competition will be explained in the cation exchange complex section (CEC).

Clay Structure and Behavior

This study will focus on the vermiculite clay due to its abundance in Fukushima Prefecture (Sano *et al.* 2010; Qin *et al.* 2012; Mukai *et al*. 2016). Vermiculite is categorized as a phyllosilicate because of its leaflike/planar structure. These structures are composed of two specific horizontal sheets: tetrahedral and octahedral sheets.
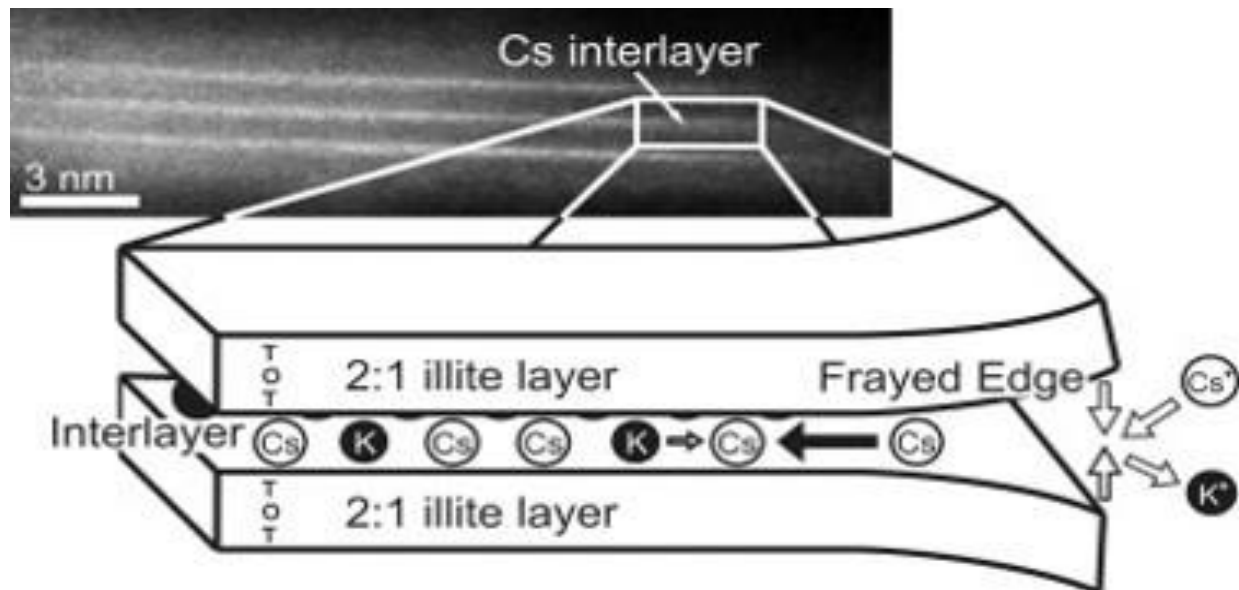
Fig. 2 – Schematic of illite clay. Illite clays differ from vermiculite in that their interlayers contain only

K$^+$ cations, whereas vermiculite interlayers are not specific to one cation. (Fuller *et al*. 2015)

Tetrahedral sheets contain two oxygen planes being held together by silicon between their spaces.

One silicon atom is surrounded by four oxygen atoms, forming a pyramid called a tetrahedron.

Octahedral sheets contain six oxygen atoms surrounding an aluminum or magnesium to form an eight-

sided geometric solid called an octahedron. Silicate clays are classified when different ratios of

tetrahedral and octahedral sheets come together. Vermiculite clays take a ratio of 2:1, meaning for

every two tetrahedral sheets there will be one octahedral sheet. In nature, the tetrahedral and

octahedral sheets experience isomorphous substitution that is responsible for the net negative charge in

silicate clays. Isomorphous substitution occurs when the central atoms found between the oxygen

atoms are substituted with atoms of a reduced charge, which shift the net charge of the clay particle to

become negative. For example, an Al^{3+} cation inside the octahedral sheet of a clay can be substituted

with a Ca^{2+} cation. The decrease from 3$^+$ charge to 2$^+$ charge signifies a reduction in the clay surface

charge causing an imbalance in the overall charge of the octahedral sheet. Thereby, a net negative charge is created on the clay surface.

With a very small particle size, clays present the highest surface being exposed for possible radionuclide adsorption. Clays have a large internal surface area between its layers of the formation that must be accounted for. Each individual sheet has its own internal surface area that adds to the total surface area of the clay. The total surface area of colloids can range from 10 m^2/g for the external portions of clay while the internal portions can contain more than 800 m^2/g. Thus, the high surface area provides ample opportunity for significant retention of cations like $^{137}Cs^+$ (Brady and Weil, 2008).

Cation Exchange Complex (CEC)

Research involving the removal of $^{137}Cs^+$ on vermiculite is centered around the attraction of cations to negatively charged clay surfaces. The sum total of all negatively charged sites where cations interact with the surface of negatively charged clay is called the cation exchange complex (CEC). Cations enter a hydrated phase that allows them to interact with the clay surfaces. The hydrated cations are in constant exchange with soil surfaces and the surrounding solutions. Cation exchange reactions involve the outer-sphere complex where water molecules form a weak electrostatic attraction between adsorbed ions and the charged colloidal surface. When adsorbed cations begin moving too far away from the clay surface, it can be replaced or exchanged by other hydrated cations. This exchange is continual, but all interactions are in equilibrium meaning there will be no further net change in the number of adsorbed competing ions (Brady and Weil, 2008). Ion charge or valency plays a key role in competition between determining which ions are being adsorbed to clay surfaces or in solution. Generally, ion selectivity has been described as $Al^{3+} > Sr^{2+} > Ca^{2+} > Mg^{2+} > Cs^+ > K^+ = NH^{4+} > Na^+ > Li^+$. Monovalent ions will be replaced by ions of higher charge unless the concentration of a monovalent ion is overwhelmingly greater than the multivalent species. It is believed that the majority of cation exchange reactions are reversible in

that the cations adsorbed to the clay surface can be removed and replaced with other cations. However, this is not always the case.

Clay Interlayers

Interlayers are the spaces that separate clay sheets. Vermiculite clay sheets are comprised of two tetrahedral and one octahedral layer as can be seen in Figure 2. As cations of reduced charge replace Al^{3+} and Si^{4+} in the octahedral and tetrahedral sheets, a surface charge imbalance is created on the external portion of the sheet. This negative surface charge must be brought back to a net zero through interactions with cations. These 2:1 sheets are thus held together through cationic interactions which are induced by satisfying the overall negative clay surface charge. The cations between the 2:1 sheets occupy the clay interlayers, therefore holding the sheets together in aggregate making various clays. Interlayer expansion is important as it determines the levels of ion exchangeability in interlayers. As interlayers expand, the spaces separating the interlayers become larger allowing cations with larger ionic diameters to interact with the CEC. Conversely, interlayers can be very small, decreasing the cation availability for adsorption. Vermiculite interlayers generally contain water molecules, K^+, Mg^{2+}, and other ions (Brady and Weil, 2008). Clay interlayers can vary in size at any given moment making it difficult to report. However, when interlayers are too small for hydrated cations to enter, some cations can dehydrate allowing them to fit in otherwise inaccessible places. When this happens, interlayer size decreases to a much smaller size than when hydrated ions exchange. The dehydrated ions close interlayers so tightly that any hydrated cations can no longer interact with vermiculite interlayers. It is theorized that due to a strong fixation in the interlayer, $^{137}Cs^+$ contaminated soils in Fukushima Prefecture are considered to have dehydrated and strongly adsorbed to vermiculite interlayers (Ferreira *et al.* 2018). This strong fixation of cations to clay interlayers can be further explained through the NISE effect.

NISE Effect

Ions are surrounded by a hydration sphere that inhibits them from adsorbing to certain areas of the mineral surface. However, a clay nanopore can have a significant effect on cation adsorption mechanisms. A nanopore can be thought of as a tunnel inside a mineral. Different minerals have different tunnel sizes, and, depending on their size, these nanopores can greatly affect the adsorption of ions. Ferreira and Schulthess (2011) proposed that an ion can shed its hydration sphere, allowing it to adsorb inside nanopores using a stronger adsorption mechanism then it could on a typical surface adsorption site. Through this mechanism, ions that are normally weakly held on the mineral surface can dehydrate and adsorb by a stronger inner-sphere mechanism. This phenomenon is called the nanopore inner-sphere enhancement (NISE) effect (Ferreira and Schulthess 2011). With systems containing small nanopores, ion adsorption and ion exchange can be greatly influenced by the NISE effect. Thus, if clay interlayers reach a size comparable to that of a nanopore, the NISE effect could be applied to vermiculite providing an explanation on how Cs^+ becomes trapped and non-exchangeable.

Frayed-Edge Sites (FES)

A vital part of clay structure involves the concept of frayed-edge sites (FES). An FES is said to form when interlayer spaces are partly expanded due to weathering. The sheets in 2:1 clays are bound to other 2:1 sheets through cationic interaction between interlayers. Weathering can slightly "peel" the FES leaving an opening for ionic interactions. This peeling back of interlayers exposes fixed cations, allowing exchangeable ions to potentially enter a collapsed interlayer and start removing adsorbed cations. It is possible that vermiculite with FES in Fukushima Prefecture was exposed to $^{137}Cs^+$. With a hydration energy of Cs^+ (287.3 KJ/mol) compared to K^+ (337.1 KJ/mol), Cs^+ should preferentially adsorb to vermiculite surfaces (Brouwer et al. 1983). An FES could be used as an entry point for competing cations which might describe a mechanism on how Fukushima Prefecture vermiculite interlayers collapsed, leaving $^{137}Cs^+$ trapped inside and non-exchangeable.

Kinetics: Adsorption and Desorption

Of interest is the kinetics at which $^{137}Cs^+$ adsorbs to vermiculite surfaces. There is insufficient literature providing the information to fully understand the adsorption kinetics of $^{137}Cs^+$ to vermiculite, promoting research to head in that direction. Using the information from a Cs^+-vermiculite adsorption envelope, it could be shown that Cs^+ binding is affected by competing ions and highly-concentrated cationic solutions. Therefore, an experiment can be set up where Cs^+ is introduced into a suspension of vermiculite and a competing cation at varying time intervals (ranging from 0-1440 hours). This would tell how quickly clay interlayers collapse and if ion competition increases or decreases the total amount of adsorbed Cs^+.

Typically ion exchange reactions on surface sites are usually expected to reach equilibrium within a matter of seconds. A study by Murota *et al*. (2016) suggests that extended periods (weeks or possibly months) of time are needed to properly evaluate the irreversibility of $^{137}Cs^+$ binding in vermiculite. However, a conflicting study has been shown that Cs sorption onto vermiculite is relatively fast (within minutes) and that once the cesium is removed it can easily re-adsorb and re-intercalate to the clay (De Koning and Comans 2004). To avoid to re-adsorption of cesium, the researchers used a cation exchange resin that would capture desorbed Cs^+ while replacing the exchange complex with K^+. Their results showed that $^{137}Cs^+$ can be removed if the soil is suspended in a strong solution of KCl for extended periods of time, a technique called the "infinite bath." As stated previously, cation exchange is affected by the concentration of hydrated cations. Thus, it would be expected that a highly-concentrated solution of KCl should displace $^{137}Cs^+$ from the cation exchange complex. However, due to the strong fixation, $^{137}Cs^+$ cannot be fully removed and replaced with other cations just by using highly concentrated cationic solutions and without the use of a Cs^+-capturing resin, Cs^+ would re-adsorb to the clay surface (Murota *et al*. 2016). The speed at which the reactions occur (i.e. in seconds (de Koning) is experimentally examined in this thesis.

Hypotheses

The available literature of Cs$^+$ interactions with vermiculite is incomplete when describing the Cs$^+$ adsorption envelope, kinetics, and total Cs$^+$ adsorption when in the presence of competing ions. It must first fully be described how Cs$^+$ binds to vermiculite surfaces to suggest effective removal methods. Knowing Cs$^+$ binding behavior could improve the understanding of ^{137}Cs$^+$ movement, the rate at which ^{137}Cs$^+$ binds to vermiculite, and the selection of chemicals for extraction of ^{137}Cs$^+$. The proposed research developed an adsorption envelope that describes Cs$^+$ binding behavior and analyzed the adsorption kinetics of Cs$^+$ binding to vermiculite. The following hypotheses were presented:

1. The adsorption of Cs$^+$ is a function of pH and will be greatly impacted by soil pH. H+ is part of the CEC reactions, but also contributes to acidity. As soil pH increases there should be an increase in total adsorbed Cs$^+$ to vermiculite surfaces. Vice versa, as pH decreases there should be a decrease in total adsorbed Cs$^+$.

2. The Cs$^+$ adsorption kinetics will show how vermiculite interlayers collapsing or becoming inaccessible, within the first five minutes of Cs$^+$-vermiculite interactions. This implies that Cs$^+$ quickly binds to vermiculite, preferentially adsorbing over other competing cations previously adsorbed.

Methods

Soil Collection and Washing

Research grade vermiculite (VWR International of Radnor, PA) was ground using a mechanical grinder to reduce the particle size to <200 μm. The vermiculite was then suspended by volume in a 0.5 M HCl solution at a 2:1 ratio and mixed for two hours. After the mixing period, a vacuum filter was assembled using a 15 μm filter paper. The suspension of vermiculite and HCl was poured into the vacuum filter, remaining there for two hours. The filtered vermiculite was then removed and resuspended in HCl to repeat the washing process two more times. This process removed as many natively adsorbed cations as possible leaving primarily H$^+$ on the cation exchange complex. When the

washing was complete, the vermiculite was completely dried before being reground to <200 μm at which point it's ready for use.

Sample Preparation

Experiment #1 - Cesium Adsorption Envelope

Samples are prepared in 35 mL centrifuge tubes. One gram of acid washed vermiculite was weighed out in the centrifuge tube. To achieve a full range of pH coverage, specified amounts of deionized water and hydrochloric acid were added to the samples (refer to Appendix). An auto-titrator (Metrohm Titrino plus 877), administered from 0-20 mL DI H_2O into the sample. Hydrochloric acid and cesium hydroxide were administered using a smaller auto-titrator (Metrohm Titrino plus 877) that delivers up to 5 mL at a time. The concentration of delivered solutions was as follows: 1.21 M HCl and 0.1 M CsOH. Using auto-titrators to deliver liquids into the system ensured consistency throughout the experiment. The order of addition was DI H_2O, HCl, and then CsOH. While the amounts of DI H_2O and HCl were delivered in varying amounts to achieve different pH levels for each sample, 14.00 mL of CsOH was delivered to all samples. Once all the solutions were mixed together, the samples were placed on a hematology mixer for 18 hours before being removed. When the mixing period was over, the samples were removed and placed in a centrifuge. Samples spun in the centrifuge for 5 minutes at 5000 rpm before increasing to 10,000 rpm for 10 more minutes. After 15 minutes of centrifuging, the samples were gently removed to avoid vermiculite re-suspending into solution. A pH probe was calibrated using 4, 7, and 10 calibration solutions. It was required that the pH probe have a calibration slope greater than 90.0% to adhere to QA/QC standards. Corresponding scintillation vials and 25 mL test tubes were labeled. From the centrifuge tube containing separated vermiculite and liquids, 5 mL of the supernatant was extracted and added to a scintillation vial and 15 mL was added to a test tube. The scintillation vial containing 5 mL of sample was used to check sample pH and was later discarded. The test tube containing 15 mL of sample was transported for analysis at an external laboratory. Solids and liquids remaining in the centrifuge tube were later discarded in a hazardous waste bin.

Experiment #2 - Cesium Adsorption Kinetics Experiment

A 0.1 M cesium hydroxide solution in combination with a 0.1 M potassium hydroxide was used to

determine the Cs adsorption kinetics on vermiculite. Samples are prepared by first weighing out 1 g of

vermiculite into a 35 mL centrifuge tube. DI H_2O and 1.21 M HCl were added using Metrohm auto-

titrators. To maintain the same concentration of K^+ and Cs^+, 14.00 mL of 0.1 M KOH was added to the

centrifuge tube. The samples were placed on hematology mixers for the following time intervals before

introducing Cs^+:

Time (hr)
0
12
24
168
336
720
1440

At the end of the mixing period, the samples were removed so that 14.00 mL of 0.1 M CsOH could

be added. After introducing Cs^+, the samples were placed back on the hematology mixer where they

were mixed for an additional 18 hours. Samples then followed the same centrifugation, extraction, and

pH measurement procedures as the Cesium Adsorption Experiment. Experimental controls containing

0.1 M CsOH and 0.1 M KOH, without vermiculite, were prepared for analysis.

Instrumentation

Birla Carbon provided the instrumentation needed to complete sample analysis. Samples were

taken to Birla Carbon and analyzed for ionic concentrations using an inductively coupled plasma optical

emission spectrometer (ICP-OES) (HORIBA Scientific, instrument model Ultima Expert). Samples were

injected into the ICP spectrometer by a peristaltic pump and entered a nebulizer which turned it into a

mist. The sample mist was then introduced directly into an argon plasma where it became ionized and

separated into its atomic components. This molecular break up causes back and forth in atoms to lose

and recombine their electrons. This process gives off radiation at characteristic wavelengths that were

then measured using specified intensity lines (Haung *et al.* 1989). QA/QC blanks were analyzed every 10 samples. The QA/QC samples represented specific concentrations of Cs^+ and K^+ to help determine the total amount of adsorbed cations on vermiculite surfaces.

Analysis

The adsorption behavior of Cs^+ onto vermiculite surfaces were examined by linear regression analysis. Cesium standards of 1,000 and 10,000 ppm (Fisher Scientific, Alfa Aesar plasma standard solution), were used to create the calibration curve. The calibration standards used in the curve were 5,000, 2,500, 1,000, and 100 ppm of Cs. The calibration curve was required to have a R^2 value greater than 0.9995 to be suitable for analysis. Data collected from the ICP-OES was obtained in parts per million (ppm), which was converted to milimolar (mM) and later millimoles per gram (mmol/g). Converting the measurement to mmol/g allowed us to interpret the amount of $^{133}Cs^+$ adsorbed to the surface of one gram of vermiculite. The following example converts a measured 1350 ppm $^{133}Cs^+$ to mM:

$$1350\ ppm = 1350\frac{mg}{L}$$

$$1350\frac{mg}{L} \times (0.001\ g\ \div 1\ mg) = 1.350\frac{g}{L}$$

Using the atomic weight of ^{133}Cs (132.90545 mol/g), mol/L (or molarity, M) can be calculated:

$$1.350\frac{g}{L} \times (1\ mol\ \div 132.90545\ g) = 0.01015\frac{mol}{L}$$

$$0.01015\frac{mol}{L} \times (1000\ mmol\ \div 1\ mol) = 10.15\frac{mmol}{L}\ or\ 10.15\ mM$$

The system has a set total of 35 mL and 1.0000 ±0.0020 g of vermiculite. Thus, mmol/g can then be calculated by:

$$35\ mL\ \times (0.001\ L\ \div 1\ mL) = 0.035\ L$$

$$0.035\ L\ \times 10.15\frac{mmol}{L} = 0.3553\ mmol$$

$$0.3553\ mmol\ \times 1.0000\ g = 0.3553\frac{mmol}{g}$$

This example allowed us to infer that 0.03553 mmol/g of $^{133}Cs^+$ adsorbed to the surface of one gram of vermiculite.   Note that during the data treatment, converting ppm to mmol/g required the mass of each individual sample where one gram represented the total vermiculite added to the sample which should be 1.0000 ±0.0020 g. The data was presented in a graph showing total adsorbed Cs in mmol/g as pH changes. The adsorption kinetics followed the same data treatment, with multiple adsorption envelopes being developed and labeled to accurately represent their corresponding time interval.

Results
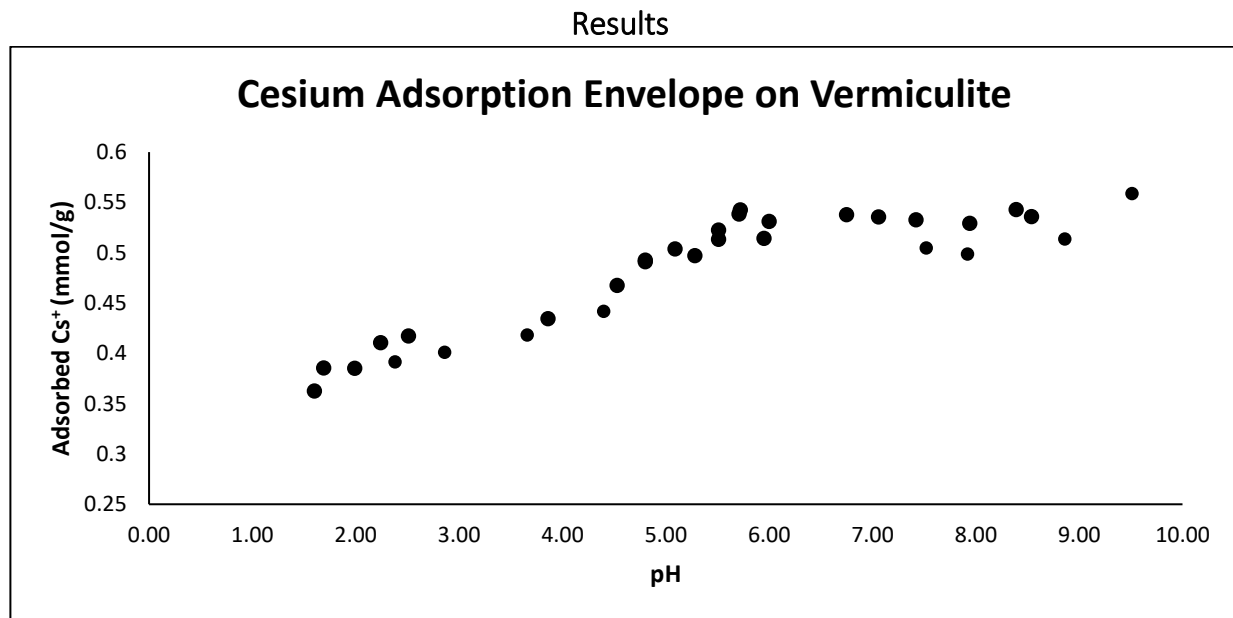
Fig. 2 – Cs^+ adsorption envelope showing how the adsorption of Cs^+ changes as a function of pH.

It can be seen in Figure 2 that as vermiculite pH increases, so too the total adsorbed Cs^+ to vermiculite increases. Likewise, as pH decreases, the total adsorbed Cs^+ to vermiculite decreases. There is a strong adsorption mechanism displayed by Cs^+ for vermiculite adsorption sites. This can be seen around pH 1.5 which shows a high concentration of H^+ is required to outcompete Cs^+ for adsorption sites.
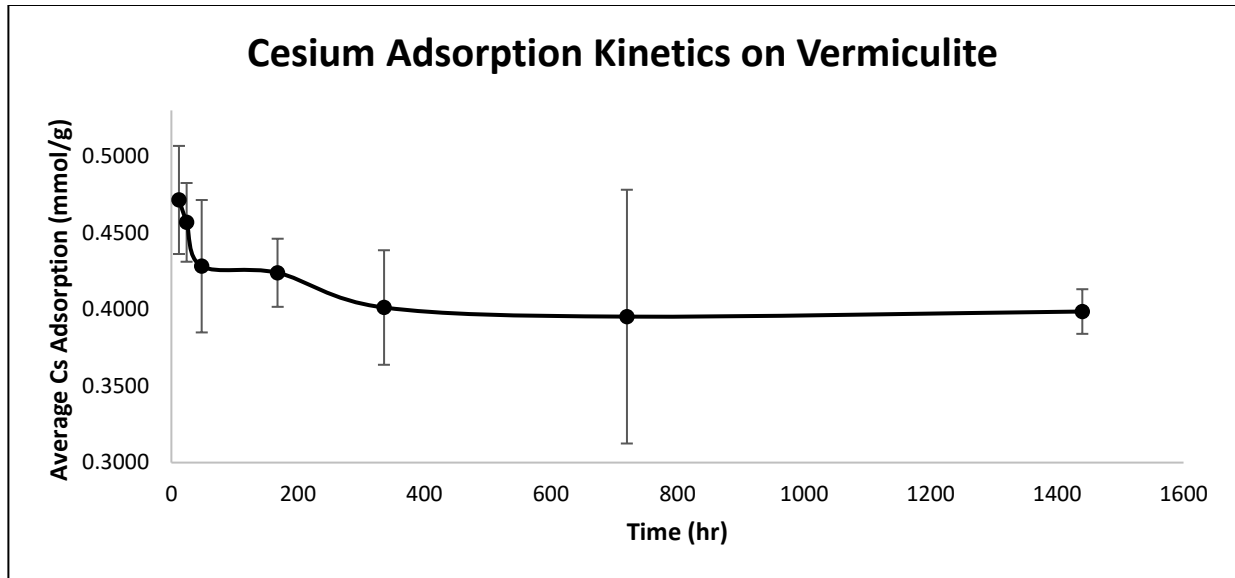
Fig. 3 – Adsorption kinetics of $^{133}Cs^+$ interaction with $^{39}K^+$-impregnated vermiculite showing the impact of K^+ equilibration time on Cs adsorption.

The adsorption kinetics of Cs^+ to vermiculite shows a continual decrease over the extended time intervals. Initially adsorbing around 0.4700 mmol/g at 12 hours, the adsorption of Cs^+ decreases to approximately 0.4000 mmol/g throughout the remaining time interval.
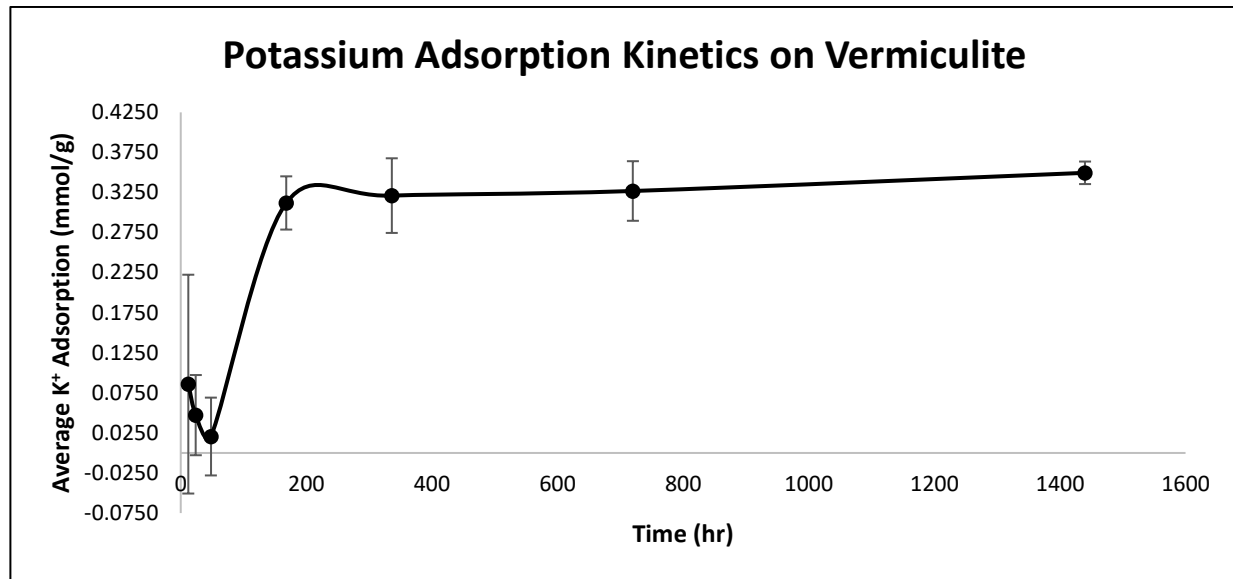
Fig. 4 – Adsorption kinetics of $^{39}K^+$ on vermiculite.

The potassium adsorption data should be evaluated with caution. Instrumental error gave a negative result for method blank in multiple trials. This method blank is used to back calculate the total adsorbed K^+ on vermiculite surfaces. K^+ was delivered to vermiculite at a solution concentration of 0.040 M. Therefore, to avoid negative values in the dataset, the calculated K^+ concentration was used to construct Figure 4. Note that the curve of the graph would not change regardless of the K^+ method blank value, only where the graph falls on the axes.

Discussion

The results of this research significantly increase our understanding of the radiocesium binding mechanisms on clay minerals in the soils of Fukushima Prefecture in Japan. The first hypothesis was that Cs^+ adsorption is a function of pH; as pH increases the total adsorbed Cs^+ will increase and as pH decreases total adsorbed Cs^+ decreases. Experimental results support the hypothesis that Cs adsorption is influenced by the solution pH and ionic strength. With Cs^+ being the only cation in the system other than H^+, an increase of total adsorption increased as pH increased. Conversely, as pH decreased the

total adsorbed Cs^+ decreased due to the higher concentration of H^+ competing in cation exchange. The adsorption envelope for Cs^+ on vermiculite shows a strong adsorption mechanism, indicating a high affinity of the vermiculite surface for Cs^+. There is an observed adsorption edge beginning around pH 3.0 moving right to left with decreasing pH. Our results show the need for high H^+ concentrations to compete with Cs^+ and affect its ability to occupy adsorption sites. This indicates a strong adsorption mechanism. In comparison, Ferreira and Schulthess (2011) used ferrierite, a nanoporous zeolite mineral known to exhibit the NISE effect which creates strong adsorption mechanisms for monovalent ions. Their results showed an initial K^+ adsorption edge around pH 4.0, whereas the initial adsorption edge for Na^+ did not start until approximately pH 5.0 (Ferreira and Schulthess, 2011). Schulthess and Huang (1990) showed sharp adsorption edges for Ni^{2+} on aluminum oxide starting at approximately pH 6.5 and for Ni^{2+} on mordenite at approximately pH 4. Adsorption of Ni^{2+} on aluminum oxide dropped to zero at pH 5 and was close to zero (approximately 10% still adsorbing) at pH 2.5 on mordenite. The comparisons demonstrate the high adsorption strength displayed by Cs^+ on vermiculite given that its adsorption edge starts at pH 3 and that the amount adsorbing is still high at a pH as low as 1. Another indication of the affinity of vermiculite for Cs^+ adsorption is that the total amount of Cs^+ adsorbing to the surface at pH 1.01 (0.35 mmol/g) is relatively high for such a low pH. This is not much of a decrease compared to the amount of Cs^+ adsorbing at pH 8.86 (0.54 mmol/g). Increasing the H^+ concentration by almost 8 orders of magnitude is only sufficient to reduce the amount of Cs^+ adsorption by approximately 35%. This shows an ability of Cs^+ to compete for adsorption sites when one considers that Cs^+ is present at an initial concentration of 0.040 M and the H^+ ions are present at a concentration of 0.1 M. At such a low initial concentration, the affinity of Cs^+ adsorption on vermiculite is favored compared the H^+, which was introduced at a much higher initial concentration.

The second hypothesis stated that the Cs^+ adsorption kinetics will show vermiculite interlayers collapsing or becoming inaccessible, within the first five minutes of Cs^+-vermiculite interactions. The

results from this experiment do indicate that vermiculite interlayers collapse that quickly. These results

disagree with a collective understanding of reaction kinetics for adsorption reactions on mineral

surfaces. Ion exchange reactions would be expected to reach equilibrium on the order of minutes, not

hours. The data indicates that after 48 hours of equilibration, the system is continuing to decrease in

the amount of Cs^+ adsorption. Figure 4 indicates that the interlayers have yet to be completely

collapsed by adsorbing K^+ as there is an observed increase in K^+ adsorption still occurring, even after

such an extended period (beyond 336 hours). There was no statistical difference reported between

time intervals. It was expected that interlayer collapse would happen much sooner than this and

believed that the adsorption affinity of Cs^+ would outcompete K^+ no matter how long the time interval of

K^+-vermiculite equilibration occurs. Thus, these results indicate that there can be no true vermiculite

interlayer collapse when K^+ is in competition with Cs^+ because Cs^+ will always find a way to adsorb to

vermiculite surfaces. These results cannot agree with the claims made by DeKoning and Comans (2004)

that suggesting interlayer collapse to occur within seconds nor can they agree with the claims made by

Murota *et al.* (2016) that interlayer collapse occurs in a time span of days to weeks. The contradictions

from these results indicate that further research into the kinetics of clay interlayer collapse of 2:1 is

warranted. However, Ferreira *et al*. (2018) showed a decrease in interlayer spacing after Cs^+ interacts

and adsorbs to vermiculite.
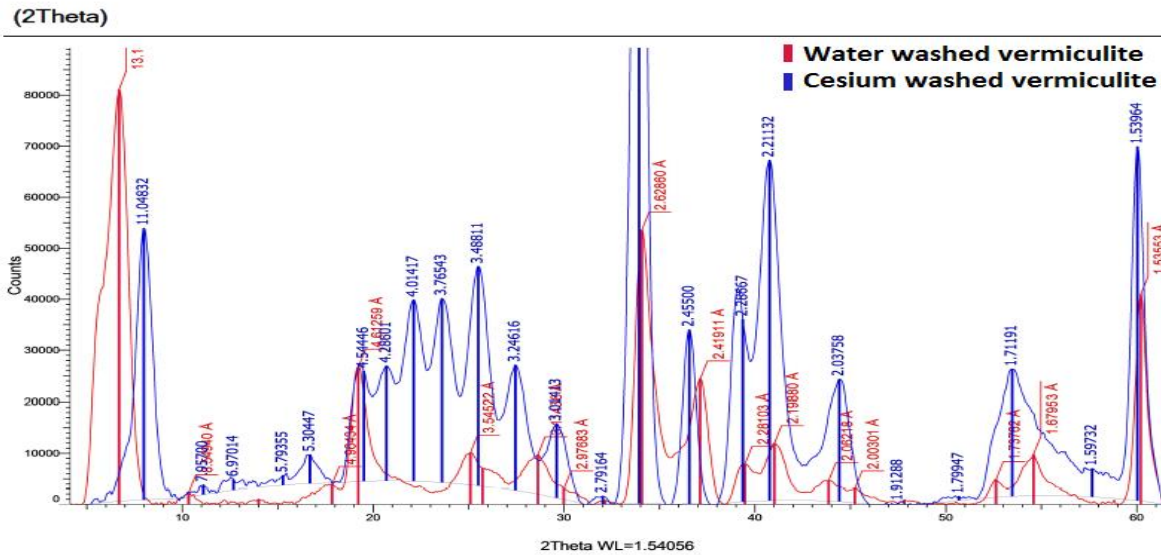
Fig. 5 – Powder XRD spectra of water washed vermiculite and cesium washed vermiculite. *(Ferreira et al. 2018)*

Powder XRD analysis showed an interlayer dimension averaging 3.25 angstroms for vermiculite equilibrated with water compared to an average of 1.20 angstroms in vermiculite equilibrated with cesium chloride (CsCl). These results suggest that adsorbing cesium ions caused the interlayer dimension to decrease over 63% (Ferreira *et al.* 2018). Given that Cs^+ is preferentially adsorbed to vermiculite surfaces, the ineffectiveness of H^+ or K^+ to compete with Cs^+ in ion exchange reactions on vermiculite was surprising. Even at high H^+ concentrations and a relatively low Cs^+ concentration as observed in figure 2, Cs^+ was still competing for adsorption sites on vermiculite. This indicates that as radiocesium settled to ground throughout Fukushima Prefecture, it had the ability to outcompete previously adsorbed cations for clay mineral adsorption sites allowing it to hypothetically enter clay interlayers and become tightly held. It is possible that the NISE effect is occurring and increasing as more Cs^+ adsorbs potentially explaining why vermiculite interlayers with adsorbed Cs^+ are held tightly together. This is concerning for contaminated areas of Fukushima Prefecture in that the NISE effect

greatly enhances the adsorption strength of cations, which presents challenges in attempting to develop soil restoration strategies as the removal of tightly held radiocesium could be very difficult. These data show that the task of removing adsorbed radiocesium from contaminated Japanese soils may be even more difficult than originally anticipated and supports the efforts of the Japanese government in removing the top 5 cm of soil.

Future Work

The results of this study provide other research opportunities. Of most importance, illite could be used to further examine the affinity of Cs^+-adsorption mechanisms. Illite is a 2:1 clay like vermiculite, but rather than having multiple cations adsorbed to its interlayers, illite contains only K^+. An experiment could be setup following a similar design to that of the kinetics experiments where illite was exposed to Cs^+ and allowed to equilibrate for varying time intervals such as 12, 48, 168, 336, 720, and 1440 hours. After the allotted time intervals samples could be taken for x-ray diffraction analysis to measure interlayer spacing compared to a control of illite not exposed to Cs^+. The results from in this thesis work indicates it would be expected that as the time intervals of Cs^+-illite interactions increase, K^+ in the supernatant would increase due to Cs^+ outcompeting K^+ for adsorption sites.

Part Two – Using Bioindicators to Evaluate Fukushima Prefecture Ecological Health

Background

The movement of $^{137}Cs^+$ contaminated clay by weathering and erosion can potentially be monitored using bioindicators. A bioindicator species is an organism whose physical appearance is interpreted as an indication of the ecosystem's health to identify specific environmental hazards. Bioindicator species can be useful for monitoring the environmental impacts of long-term radiation exposure on Fukushima Prefecture caused by the meltdown of the FDNPP. This approach to ecosystem monitoring appeals to ecologists as it is a low cost and time efficient method for evaluating environmental disturbances (Carignan and Villard, 2001). Using bioindicator species to monitor the movement of artificial radionuclides through ecosystems would benefit Fukushima Prefecture for several reasons. First, bioindicators are low cost in comparison with technological devices such as Geiger counters or dosimeters. The availability and low cost of bioindicators will allow residents to ensure that contaminated clay is not being transported into previously remediated areas through erosion. Second, there would be little to no required training for the bioindicators. Methods involving radionuclide analysis technology require technical training, such as calibration or maintenance of electronic devices, which can be complicated. Finally, the ease of planting would allow residents to plant in many areas, including uninhabited areas. Monitoring the bioindicators requires very little effort, allowing individuals to make quick visual inspections of the plants' health. The intent of this study was to use bioindicators in Fukushima Prefecture to evaluate ecosystem health and predict, if any, ecological consequences resulting from FDNPP artificial radionuclide exposure while also evaluating to the bioindicators species as potential phytoremediation candidates.

Evidence for Bioindicators in Fukushima

A study conducted by Watanabe *et al*. (2015) presented evidence of coniferous trees experiencing morphological abnormalities in the Fukushima area. Coniferous trees have been used to evaluate

artificial radionuclide's impact on ecosystems by observing abnormalities such as main axis branching (Sparrow and Woodwell, 1962; Sparrow *et al*. 1965; Ohba, 1964). Fukushima has an abundance of the Japanese fir, *Abies firma*, which serves as a convenient bioindicator species because young trees are short enough for an easy observation of morphological changes and tree branching. The authors established their study on three sites near FDNPP which ranged in ambient radiation exposure. A control was established 400 km south of Fukushima Prefecture in Kyoto where artificial radionuclides released from FDNPP are below the limit of detection. Observed defects in *A. firma* were characterized by irregular branching at the main axis with a distinct deletion of the leader shoot which would normally elongate to form the main axis and be filled in with remaining branches. Their results found a significant increase in *A. firma* defects growing near FDNPP in comparison with the population in Kyoto. Furthermore, the frequency of morphological abnormalities corresponded with the locale of sampling. As ambient dose increased, the number of abnormalities increased, suggesting that exposure to higher artificial radionuclides can increase tree deformities (Watanabe *et al.* 2015). Supporting evidence was presented in Chernobyl where Scots pine trees chronically exposed to artificial radionuclides also showed a deletion of the leader shoots (Kozubov *et al*. 2007).

Possible Mechanisms for Cs Uptake

The mechanism by which Cs^+ is taken up by plants roots is not completely understood. It is known that plants can readily absorb and translocate Cs to their above-ground plant parts where Cs is then mainly concentrated in tissue. However, Cs absorption by plant roots is less efficient than K (Menzel and Heald, 1995). Among all alkaline metals, K^+ competes most with Cs^+ uptake inhibiting plants' ability to uptake Cs^+ in areas with higher concentrations of K^+. There is a body of research suggesting that lowering K^+ concentration increases the amount of Cs^+ uptake (Shaw and Bell 1991; Shaw et al. 1992; Zhu and Shaw 2000). As K^+ concentration was decreased in nutrient solutions, Cs^+ uptake by plants was

greatly increased (Cline and Hungate 1960; Nishita *et al*. 1962). The actual concentration for K^+ was not reported in these studies.

Nissen (1991) proposed that K^+ carrier and channel modes were possible mechanisms for routes of Cs^+ uptake in plants. Of the carrier-mediated transporters, HKT1 was found responsible for K transport across the plasma membrane and against the electrochemical gradient (Maathuis and Sanders, 1994; Schachtman and Schroeder, 1994). Schachtman and Schroeder (1994) also proposed that HKT1 had an ion selectivity sequence of $K^+ > Cs^+ > Rb^+ > Na^+ > NH_4^+$ suggesting that in the absence of K^+, Cs^+ would be next in line for transport to plants. Supporting evidence for the ion selectivity of HKT1 was provided by Grassmann *et al.* 1996 where Cs^+ was shown to be transported at 86% of the rate of K^+ at equal concentrations of 1 mM in *Xenopus* oocytes. It has been suggested that K starvation could induce the expression of HKT1 and other K^+ transporters, potentially increasing the amount of Cs^+ uptake (Wang *et al.* 1998). Zhu *et al*. 2000 would later show a dramatic increase in radiocesium uptake in wheat after the plants had been removed from a K growth medium for three days. Of the channel-mediated transporters, the KAT1 channel was identified to be a voltage-dependent inward rectifying K^+ channel that operates at high K concentrations with an ion selectivity of $K^+ > Rb^+ > Na^+ > Cs^+$ (Schachtman *et al.* 1992). The channel-mediated transporter is a low-affinity system which operates when external K^+ concentrations are higher than 0.5-1 mM (Maathuis and Sanders, 1997). However, the KAT1 channel can be blocked by Cs at carrier concentrations of 1 mM Cs^+ rendering the channel useless in the uptake of Cs (Becker *et al*. 1996).

Plant species that can be used as bioindicators must be able to withstand high radiation exposure to in order to elucidate the long-term effects of gamma radiation on biological organisms. Research into the use of plants as bioindicators in the Chernobyl area yielded two plant species that could serve as candidates for a field trial Fukushima Prefecture. Common ferns (Shcheglov *et al.* 2013; Holm 2006) and lilies (Shcheglov *et al.* 2013; Holm 1997) were the best bioindicators of $^{137}Cs^+$ contamination of soil near

the site of the Chernobyl disaster due to their ability to uptake and withstand higher amounts of radiocesium. Shcheglov *et al*. (2013) found that the ability of bracken ferns (*pteridium aquilinum*) and may lilies (*convallaria majalis*) to accumulate $^{137}Cs^+$ in the Chernobyl soil was nearly an order of magnitude higher than the next most effective species. They reported that bracken ferns and may lilies were capable of maintaining their bioindicator properties even at an observed high radiocesium uptake, although the specific bioindicator properties were not mentioned in the study. Thus, using bracken ferns and may lilies in a natural environment should occur due to their ability to withstand high gamma radiation exposure and their potential for bioindication. The way radiation influences plant growth and development is still unknown due to varying doses of gamma-irradiation causing different degrees of morphological and structural changes (Win *et al*. 2007). Bioindicators success can be evaluated by morphological changes such as varying height and number of leaves, and a yellowing leaf discoloration caused by radiocesium uptake (Cline and Hungate, 1960; Lamseejan *et al*. 2000).

A possible challenge in attempting to use the same bioindicators in Fukushima Prefecture is that the ability of the plants to indicate the presence of radiocesium varies in different soils. Use of bioindicators could be a complicated process in environments where radiocesium is tightly bound to soil minerals and less available for plant uptake or ion exchange processes. Previous attempts made to phytoremediate the Cs in the soil in Fukushima Prefecture were considered unsuccessful, with the strength of Cs^+ adsorption to 2:1 clay minerals in the soil largely being blamed for this failure (Kobayashi *et al.* 2014). However, bracken ferns and may lilies were not used. The bioindicators may be able to take up the less tightly bound fraction of radiocesium in the soil, but radiocesium that is trapped in the clay mineral interlayers would be unavailable for uptake by the plants. The sensitivity of these specific bioindicators may allow for visual signs of distress, even with low levels of radiocesium uptake.

Hypotheses

1. The bracken ferns and may lilies will uptake radiocesium from the soil of Fukushima Prefecture. This uptake will cause observable changes in the average height, average number of leaves, and a yellowing leaf discoloration in the bracken ferns and may lilies that can be correlated to radiocesium uptake.

2. The bracken ferns and may lilies will uptake higher than 3.0 radiocesium Bq/kg as shown by Shcheglov *et al*. (2012), suggesting their effectiveness to be used as future phytoremediators. While this is not a significant amount of radiocesium being removed from soil, it is an effective long-term strategy for radiocesium removal.

Methods

Soil Collection and Planter Preparation

Bracken ferns and may lilies were purchased from a local nursery in Ikuta, Japan. The soil was collected from three different areas in Iitate Village, Fukushima Prefecture. Iitate Village is directly outside the exclusion zone that was established by the Tokyo Electric Power Company after the FDNPP accident. Radiation levels inside the exclusion zone are considered too high for residency and requires specific radiation protection gear and special permission to enter. Thus, the bioindicator project used soil from Iitate Village where the highest contaminated soil could legally be collected. The areas chosen represented various levels of radioactivity with the following radiation levels:

- Low contamination (approximately 0.5 µSv/hr)

- Medium contamination (approximately 1.5 µSv/hr)

- High contamination (approximately 3.5 µSv/hr)

The soil was then transported to the Meiji University, Ikuta Campus, for plant growth and monitoring. Before planting, the soil was filtered through a 60 mesh sieve to remove coarse organic detritus, rocks, and other bulk materials. Eighteen planters were washed to remove any previous materials, residues,

and remove as many foreign ions as possible. The planters were then labeled to represent the plant species and corresponding radiation level. Each plant species was set up in triplicate per radioactivity contamination levels for a total of nine planters per plants species. Triplicates were established to elucidate the effects of gamma radiation exposure and guarantee a high enough mass for gamma spectrometer analysis.

Growth Period

Each plant species was placed in an area that would yield at least eight hours of sunlight per day. The plants were watered occasionally to maintain a "wet-to-the-touch" soil moisture without overwatering. This equated to plants being watered roughly every three to four days. Fertilizers were not added throughout the growth period to promote potassium starvation and cesium uptake. Pictures of the plants were taken two-three times a week to elucidate the effects of long-term gamma radiation exposure. While in Iitate Village, wild bracken ferns were observed and photographed. The wild bracken fern showed no signs of morphological alterations or damage from excess radiation exposure. It was also later confirmed that may lilies were not native to Fukushima Prefecture.

Results

Figures 6 and 7 provides picture of the plants taken throughout their growth period from June-December 2017. The front row (closest to the bottom of the picture) is low-level radiation soil at 0.50 μSv/hr. The second row has a medium radiation level of 1.50 μSv/hr. The third row (closest to the top of the picture) has a high radiation level of 3.50 μSv/hr. All bracken ferns died due to excess heat exposure inside the Meiji University greenhouse. The planters were re-potted using bracken ferns taken from around the Meiji University campus. The ambient radiation levels were ~0.00 μSv/hr ensuring that no cross contamination occurred.

Plant Species #1 – Bracken ferns

Fig. 6 – Bracken ferns planted to show morphollogical changes due to radiocesium exposure and uptake. Bracken ferns were planted in the Meiji Univeristy greenhouse. Due to excessive heat, the initial bracken ferns died within two day. Bracken ferns were then repotted and moved to a location with less heat exposure.

2017-07-17

2017-07-18

2017-07-19

2017-07-26

2017-07-27

2017-07-30

2017-08-02

2017-08-04

2017-08-07

2017-08-09

2017-08-16

2017-08-17

34

2017-08-20

2017-09-04

2017-09-11

2017-09-19

2017-09-22

2017-09-25

2017-09-27

2017-11-11

2017-11-15

2017-11-18

2017-11-23

2017-11-27

2017-11-30

Plant Species #2 – May lilies

Fig. 7 – May lilies planted to show morphollogical changes due to radiocesium exposure and uptake.

May lilies were planted at Meiji Univeristy.

2017-07-26

2017-07-27

2017-07-30

2017-08-02

2017-08-04

2017-08-07
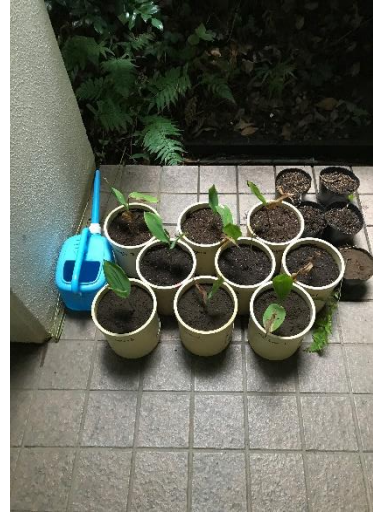
2017-08-09

2017-08-16

2017-08-17

2018-08-20

2017-09-04

2017-09-11

2017-09-19   2017-09-22   2017-09-25

2017-09-27   2017-11-11   2017-11-25

Discussion

The hypothesis that bracken ferns and may lilies, after absorbing radiocesium from the soil of Fukushima Prefecture, would have observable morphological changes in average height and average number of leaves in the bracken ferns and may lilies was not supported. The bracken ferns and may lilies did not show any signs of morphological alterations throughout the growing period and very closely resembled their respective controls. These results provide supporting evidence for Wi *et al*. (2007) who claimed that at relatively low doses (1-5 Gy) of gamma radiation there are negligible morphological changes in plants. Note that a Gray (Gy) is used when radiation exposure causes deterministic effects whereas a Sievert (Sv) is used to express dose quantities. However, 1 Gy is equivalent to 1 Sv (Annals of ICRP, 2007). This applies to the results in this study due to relatively low radiation the plants were exposed to throughout over the six month growth period:

- Low contamination = 0.00219 Sv (0.00219 Gy in deterministic effects) over six months

- Medium contamination = 0.00657 (0.00657 Gy in deterministic effects) Sv over six months

- High Contamination = 0.01533 Sv (0.01533 Gy in deterministic effects) over six months

Both plant species were exposed to considerably low gamma radiation levels and therefore should not have any observable morphological changes at such low levels. However, there was an observed yellow discoloration in the leaves which could come from radiocesium uptake as suggested by Cline and Hungate (1960), but the discoloration could also occur from lack of nutrients such as calcium, nitrogen, and potassium. It could not be determined if the discoloration was a directly correlated with radiation exposure and uptake from observations. Therefore, the plants are being analyzed for total radiocesium uptake and the growing medium should be measure for total nutrient concentration. If the plants contain elevated levels of radiocesium then the yellow discoloration in the leaves could possibly be correlated to radiocesium toxicity.

The second part of the experiment would collect the plants for total radiocesium analysis. The plants were harvested in December 2017 and are currently undergoing analysis for radiocesium uptake using a gamma spectrometer (Princeton Gamma-tech Instruments, IGC1619SD-NAIG) at Meiji University, Ikuta Campus. This project provided the opportunity for international collaboration with a Japanese university. Through interactions with graduates and undergraduates, it was agreed who would collect the soils, set up the plant trials, monitor and photograph the plants throughout the growth period, and harvest/analyze the results. It's important to note that citizens of Iitate Village had extensive training in methods of radionuclide analysis. This goes against the assumption that citizens were not adequately trained to understand the magnitude of long-term radiation exposure. Throughout Iitate Village there were numerous dosimeters actively monitoring radioactivity levels to keep citizens informed. International collaborators state that the training and equipment was provided by the Japanese government as part of its post-FDNPP accident awareness program. However, citizens are welcoming to science projects that intend to improve soil conditions in Iitate Village. The team interacted with citizens of Iitate Village who were more than willing to accommodate science projects intending to improve soil conditions. Citizens of Iitate Village were very conscious of current conditions,

having been extensively trained by the Japanese government and academics on the use of monitoring technology and good health practices.

Future Work

The plants were harvested in December 2017 and are currently being analyzed for radiocesium uptake using a gamma spectrometer. Plant roots, shoots, and stems will be combined for the plant species of each contamination level. For example, all plant parts from the three samples of low contamination bracken ferns will be combined for gamma spectrometer analysis due to mass requirements. Results from the gamma spectrometer analysis provided information that can be used to determine if the bracken ferns and/or may lilies could be used as a phytoremediation source. If either plant species yields a comparable $^{137}Cs^+$ uptake reported in the Shcheglov *et al.* (2013) study, then a future phytoremediation experiment will be established inside Iitate Village with soil that has yet to be remediated. A second experiment should be created to test for the long-term effects of plant genetics. Using a control bracken fern and may lily that has not been exposed to radiation, samples from the low, medium, and high contaminated bracken ferns and may lilies could be analyzed for cell comparison. This experiment would validate the ability of gamma emission to cause cellular and DNA damage on biological organisms while bringing awareness to Iitate Village citizens of the threats posed by long-term radiation exposure.

Acknowledgements

Japanese counterparts. Research was conducted under the supervision of Kosuke Noborio, PhD, of the

Meiji University School of Agriculture.

Part Three – Radiocesium Extraction from Fukushima Prefecture Soils Using Mg^{2+} Ions and a Cs-Capturing Ligand

Background

The highest levels of contamination are limited to an area approximately 100 square miles in proximity to Fukushima Daiichi nuclear power plant (Yasanuri *et al*. 2011). A thorough investigation revealed that that radiocesium is fixed in the top 5 cm of soil within the interlayers of the phyllosilicate clay vermiculite (Qin *et al.* 2012). With a half-life of 30.2 years, radiocesium presents a significant hazard to Fukushima Prefecture and its affected citizens for the foreseeable future. A sizable portion of research indicates that, without dissolving the clay mineral, Cs$^+$ adsorption to certain 2:1 clay minerals is irreversible (Sawhney 1964; Sawhney 1972; Comans and Hockley 1992; Fuller *et al*. 2015; Dzene *et al*. 2015). The non-exchangeable radiocesium is difficult to remove through chemical extraction, and it is believed that any type of ion exchange technique would not be an effective strategy. With this knowledge, the Japanese government decided that the top 5 cm of soil would be removed, stored and replaced. Due to the overall quantity of contaminated soil and the amount of time required for storage, remediation strategies must be explored. If a chemical extraction method can be developed remove the radiocesium from the clay portion and transfer it into the aqueous phase, the radiocesium could then be concentrated and disposed of more easily. The implications of such a chemical extraction method may have the potential to restore Fukushima Prefecture soil allowing it to be re-used.

Evidence for Chemical Extraction

Tamura *et al*. (2015) have developed a method capable of chemically extracting and removing non-exchangeable Cs$^+$ from a vermiculite interlayers by combining an ion-exchange reaction between Cs$^+$ and Mg^{2+} with a precipitation reaction. The precipitation reaction involves the use of an organic ligand called tetrakis (4-fluorophenyl) borate (TFPB) that will form a precipitate with Cs$^+$ ions, but not with Mg^{2+} ions. By adding Mg^{2+}, this allows for the removal of Cs$^+$ ions inside the vermiculite interlayer through a traditional ion-exchange reaction. Ordinarily, since the equilibrium of that reaction favors Cs$^+$, which is

preferentially adsorbed by vermiculite, the exchanged Cs^+ ions would simply re-intercalate to the adsorption site and displace Mg^{2+} back into solution. Thus, an ordinary ion-exchange based remediation solution, even involving Mg^{2+} ions that can access the vermiculite interlayer, would not work. By including the second reaction the situation changes in favor of the Mg^{2+} ions. The TFPB ligand is a large complex molecule that can form an insoluble precipitate with Cs^+, but not with Mg^{2+}. As soon as a Cs^+ ion enters the bulk solution, a TFPB molecule will bond with it and form a solid precipitate. Once the Cs^+ has precipitated, it is no longer able to participate in ion-exchange reactions, making it impossible for it to desorb the Mg^{2+} ion that replaced it inside the vermiculite interlayer. With the addition of the TFPB the Mg^{2+} ions can now remove the Cs^+ ions from vermiculite permanently. Tamura *et al*. (2015) confirmed that this method was able to remove Cs^+ ions from a pure phase vermiculite clay that they had created in the lab by saturating it with Cs^+ ions both by measuring the concentration of Cs^+ in the clay and precipitate as well as by demonstrating the re-expansion of the vermiculite interlayer using XRD indicating the removal of Cs^+ and introduction of Mg^{2+}. The work in this thesis extends the research completed by Tamura *et al*. (2015) by using TFPB on soil collected from Iitate Village.

Mechanisms of the Cs^+-Capturing Ligand

The proposed functionality and behavior of TFPB is derived from research conducted on weakly coordinated anions (WCA), which are used to describe anions that weakly interact with cations. Of interest to this thesis is the structural comparison that can be made between TFPB and anions comprised of a boron base and fluorine-containing constituents to the phenyl groups. These anions were examined and denoted BArF's (Nishida *et al*. 1984; Carreras *et al*. 2017). Carreras *et al*. (2017) described the spatial atomic arrangement and distances of the coordination bonds in BArF compounds while interacting with the alkali metals Li^+, Na^+, K^+, Rb^+, and Cs^+. The alkali metals form a compound with BArF through coordination bonds around the cationic metal alkali atom. Their study showed that different charge densities in alkali metals, arising from varying cationic radii, enable a different number

of interactions between the fluorine atoms of BArF. Cesium, having the largest atomic radii, formed

CsBArF through 14 fluorine interactions compared to the 9 fluorine interactions observed in KBArF and

RbBArF (Carreras *et al*. 2017). Cesium is the least electronegative element which would explain this

strong attraction and high number of interactions with heavily fluorinated anions.

Assuming TFPB follows a similar behavior, their results would describe the high selectivity of TFPB

for Cs^+. With its larger atomic radii, it is theorized that Cs^+ would outcompete other alkali metals for

TFPB compound formation. This theory is supported by Tamura *et al.* (2015) when TFPB was evaluated

side by side in $Cs(NO_3)$ and $Mg(NO_3)_2$. A white precipitate was formed in the $Cs(NO_3)$ solution, whereas

no precipitate was formed in the $Mg(NO_3)_2$ solution suggesting TFPB has a high affinity for elements with

little to no electronegativity. Furthermore, this thesis completed preliminary evaluations of the TFPB

cation selectivity in solution with $Ba(NO_3)_2,$ CsOH, $CaCl_2$, KOH, $Mg(NO_3)_2$, and NaOH. Results from this

evaluation showed little to no precipitation with Ba^{2+}, Ca^{2+}, K^+, Mg^{2+}, and Na^+ while showing a

tremendous amount of precipitation in the presence of Cs^+.

Hypothesis

In this experiment the research completed by Tamura *et al*. (2015) is extended by using TFPB on soil

collected from Iitate Village, Fukushima Prefecture. Dr. Tamura, through email communications,

confirmed that his extraction method was not successful when using bulk soil from Fukushima

Prefecture. This could be due to organic material interfering with the effectiveness of Mg^{2+} or TFPB.

Thus, the following hypothesis was explored in this experiment:

1. Fukushima Prefecture soil can be separated into its components where the clay portion can be

    isolated and collected. From there, the organic material can be removed from the clay and the clay

    fraction can be effectively treated with Mg^{2+} and TFPB to remove radiocesium.

Methods

Materials

    Soil samples were collected from Iitate Village, Fukushima Prefecture, Japan. At the time of

collection, radiation levels at the surface of the soil were measured at ~3.50 μSv/hr. Approximately 25

kg of surficial soil was collected and placed in a tarp bag, which was shipped from Fukushima City to

Meiji University in Kawasaki for subsequent use in the chemical extraction experiment. The soil was air

dried overnight and then was sieved through a 60 mesh (250 microns) soil sieve to remove coarse

organic detritus such as leaves, needles, rocks, excess roots.

Clay Separation and Desorption Experiments

    Using the filtered soil, 40.0 g ± 0.50 g was pulverized to achieve a uniform particle size. The soil

contents were suspended in a 5% sodium hexametaphosphate solution overnight to complex with soil

organics and promote the breakdown of soil aggregates. The samples were then diluted with DI water

and thoroughly mixed before equilibrating again overnight. The sand and silt fractions were allowed to

separate gravimetrically according to differential settling rates for particles of different sizes described

by Stoke's Law. The supernatant solution containing the clay portion and water-soluble organics was

extracted using a peristaltic pump and oven dried overnight. Samples were separated individually and

washed with multiple methanol (a common organic solvent) and water treatments to remove the

organic fraction. Approximately 3.00 grams of *untreated* clay was collected after the separation.

Samples were separated into two categories: 1) 0.50 g *untreated* soil per sample, and 2) 0.50 gram to be

treated with TFPB. This separation enabled a before and after comparison between the *untreated* and

treated clay.

    From there, 15 mL of 0.01 M tetrakis(4-fluorophenyl) borate sodium salt was mixed with 0.5 g of

the soil to complex with any $^{137}Cs^+$ entering the aqueous phase. To induce an ion exchange reaction

with $^{137}Cs^+$, 25 mL of 0.5 M $Mg(NO_3)_2$ was added to enter the clay interlayer. 10 mL DI H_2O was added,

and the samples were mixed for two hours. The clay portion was separated using a vacuum filter and

subsequent triplicate methanol wash to remove any $^{137}Cs^+$-precipitate. The portion left on the filter paper was collected, dried, and denoted as *treated*. Approximately 0.35 g treated clay was collected for analysis.

Analysis & Instrumentation

Radiation levels in trials 1 and 2 were quantified using a gamma spectrometer (Princeton Gamma-tech Instruments, IGC1619SD-NAIG) on the Meiji University, Ikuta Campus. Calibration standards containing $^{134/137}Cs^+$ were used prior to sample analysis. Due to the relatively small sample size, each sample was subjected to 50,000 seconds (14 hours) gamma spectral counting for three passes requiring 42 hours per sample being analyzed. Afterwards, the three passes were required to obtain total radiocesium contamination. Each trial required 7 days for analysis.

Untreated and *treated* samples from trial #3 were sent to Southwest Research Institute (SwRI) for total Cs^+ analysis using two analytical techniques. Samples labelled *untreated* and *treated* were analyzed via x-ray diffraction (Siemens Kristalloflex 805 with a D500 Goniometer) using a random mount orientation. The XRD spectra obtained with d-spacing scale, including the XRD library pattern matches, can be found in the SwRI report located in the Appendix. Aliquots of the soil samples (approximately 100 mg) and water sample (approximately 2.50 g) were readied for ICP-MS (Perkin Elmer DRCII ICP-MS) analysis via an open vessel, mixed acid digestion using nitric, perchloric, hydrofluoric, and hydrochloric acids. The resulting digestates for the eight soil samples contained residues. The residues were separated, dried, and fused with a lithium metaborate/tetraborate mixture.

Results

Three trials of the chemical extraction experiment were completed. Total radiocesium concentration was compared between untreated clay and clay treated with TFPB. Instrumental error has led to confusion about the authenticity of the following results. After analysis, the results indicated that the *treated* samples increased in radiocesium concentration. Since no extra radiocesium was

introduced into the *treated* samples, it was assumed that the labels were accidentally switched. Therefore, the following results are presented as if the sample labels have been switched. Conclusive results are subject to change depending on the investigation outcome.
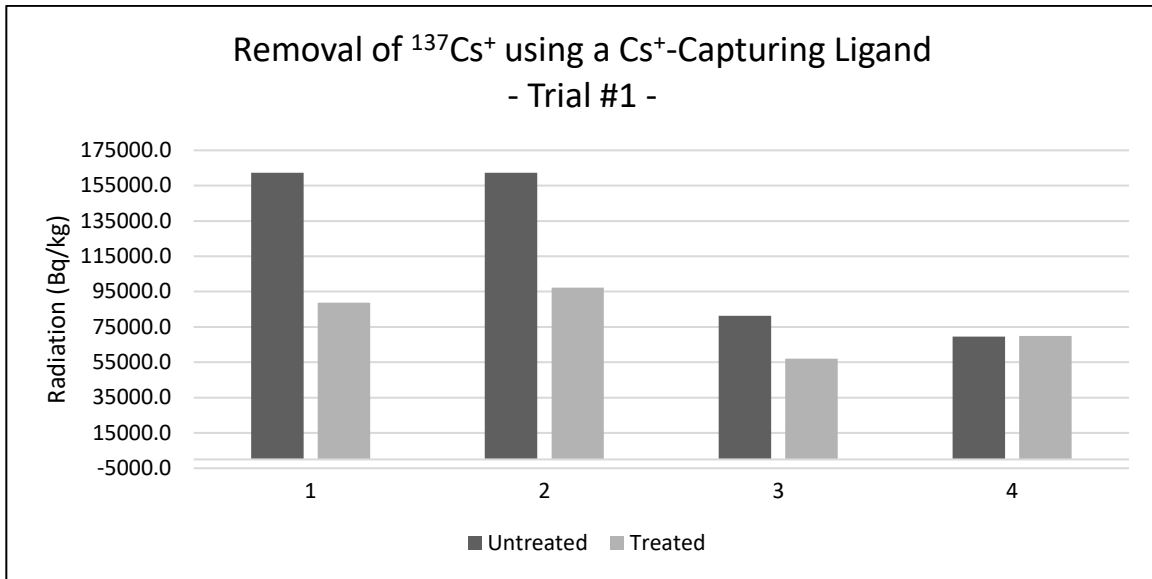
Fig. 8 – The comparison of untreated clay versus treated clay using ion exchange with Mg^{2+} and a Cs^+-capturing ligand. Gamma spectrometer analyzed for total $^{137}Cs^+$ concentration. Sample 1 decreased in $^{137}Cs^+$ by 45.35%. Sample 2 decreased in $^{137}Cs^+$ by 40.10%. Sample 3 decreased in $^{137}Cs^+$ by 29.94%. Sample increased in $^{137}Cs^+$ by 0.42%. The experiment was conducted at Meiji University, Ikuta Campus.
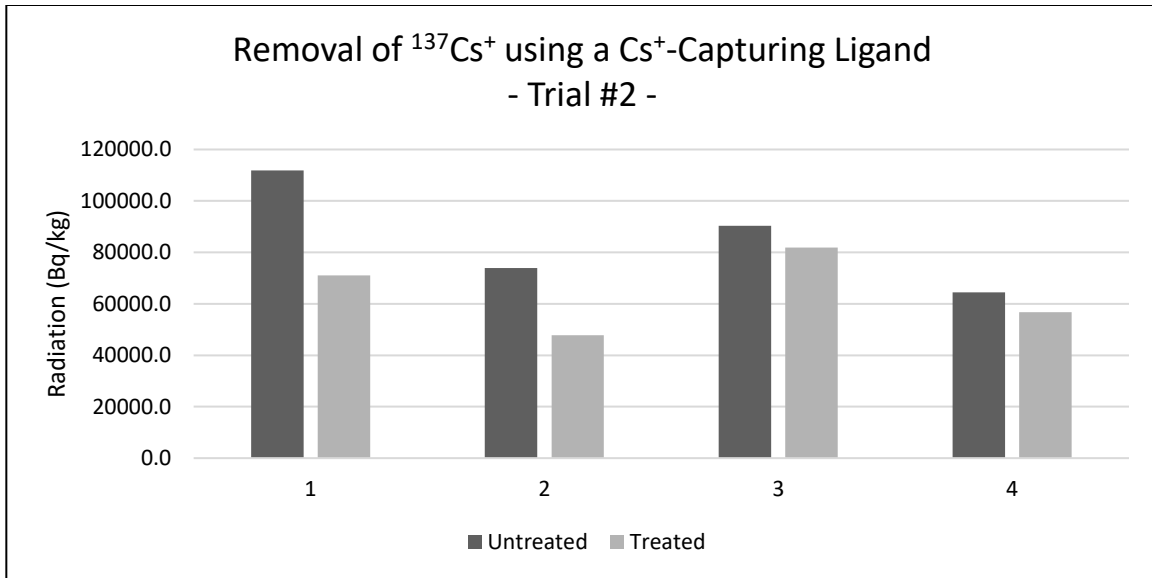
Fig. 9 - The comparison of untreated clay versus treated clay using ion exchange with Mg^{2+} and a Cs^+-capturing ligand. Gamma spectrometer analyzed for total $^{137}Cs^+$ concentration. Sample 1 decreased in $^{137}Cs^+$ by 36.43%. Sample 2 decreased in $^{137}Cs^+$ by 35.33%. Sample 3 decreased in $^{137}Cs^+$ by 9.33%. Sample decreased in $^{137}Cs^+$ by 11.97%. The experiment was conducted at Meiji University, Ikuta Campus.
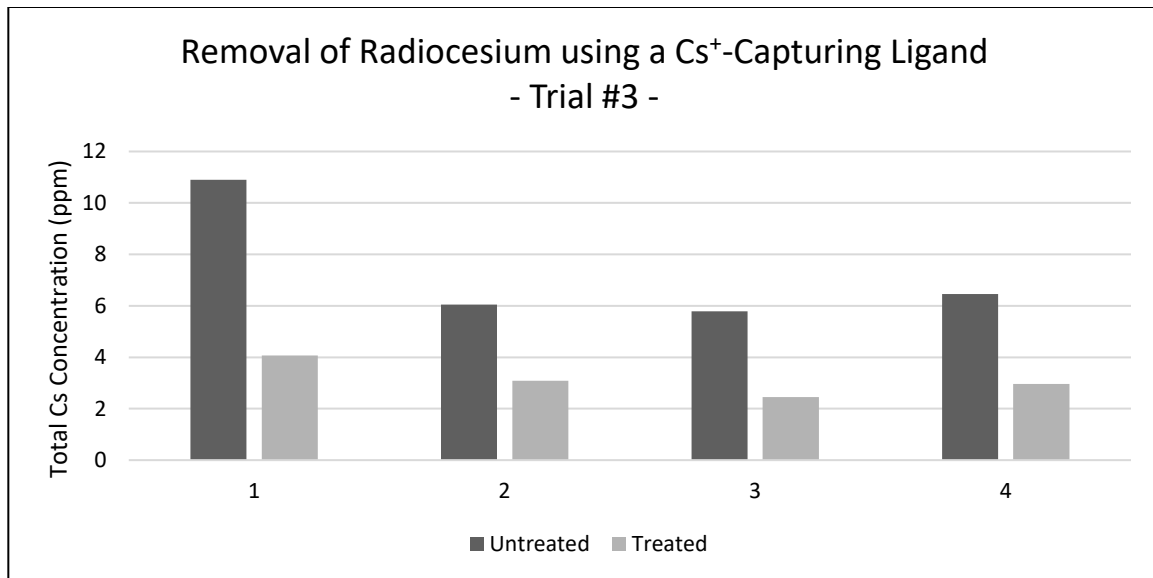
Fig. 10 - The comparison of untreated clay versus treated clay using ion exchange with Mg^{2+} and a Cs^+-capturing ligand. ICP-MS analyzed for total radiocesium concentration. Sample 1 decreased in radiocesium by 62.66%. Sample 2 decreased in radiocesium by 48.93%. Sample 3 decreased in radiocesium by 57.61%. Sample decreased in radiocesium by 54.18%. The experiment was conducted at Kennesaw State University, Kennesaw Campus.

Discussion

The results from trials 1-3 supports the ability of TFPB to remove radiocesium through a precipitation reaction, inhibiting radiocesium from re-binding and re-intercalating to clay surfaces. This radiocesium-precipitate most likely occurred due to a strong electronegative attraction of TFPB for radiocesium. As shown by Carreras *et al.* (2017), weakly coordinating anions, specifically boron based with fluorinated phenyl groups, exhibits a strong attraction towards Cs^+ due to its electronegative position. TFPB, with its boron base and its four surrounding fluorinated phenyl groups constitute a relatively high electronegativity. In the presence of a low electronegative element, TFPB should preferentially attract and bind with radiocesium. The study results provide evidence for this hypothesis. It is important to restate the need for removing organic material prior to introducing TFPB. Tamura *et*

al. (2014) experienced a shortcoming while transferring their method to soil from Fukushima Prefecture. Through email communication, Dr. Tamura confirmed that his method did not work using Fukushima Prefecture soil. It is possible that their extraction protocol did not properly isolate the clay fraction of the soil, which could interfere with the effectiveness of Mg^{2+} to exchange the interlayer Cs^+ or with the effectiveness of TFPB to precipitate with radiocesium. The extraction method in this thesis established that the clay fraction must be properly isolated to avoid TFPB interference. This deviation required extra materials and methods; however, the results indicate that separating the clay fraction and removing organic material promotes the ability of Mg^{2+} and TFPB to remove radiocesium from Fukushima Prefecture soil.

Future Work

Future work will be focused on improving the extraction experiment. Due to radiocesium remaining in the *treated* samples, it is possible that radiocesium-precipitate was not adequately removed calling an extensive methanol rinse. In previous trials, *treated* clay was washed three times with methanol to remove radiocesium-precipitate remaining in the system. Experimental results from previous trials indicate that this is not sufficient. Future trials will re-suspend the treated clay in methanol for two hours, where it will then be vacuum filtered and repeated for a total of six methanol washes to ensure radiocesium-precipitate removal. The six methanol washes will then be sent for total radiocesium analysis alongside *untreated* and *treated* samples. In theory, total radiocesium concentration in the methanol washes should add up to the difference between total radiocesium concentration in the *untreated* and *treated* samples. The structure of the precipitate should be determined using X-ray analysis to elucidate the molecular geometry of the radiocesium-precipitate. Crystals for analysis could be hard to obtain as the white precipitate was very fine under normal laboratory settings. A proposed method for acquiring large enough crystals from the precipitate are beyond the purview of this thesis and would require a greater knowledge of crystallography than can be provided by the author.

While TFPB presents compelling evidence for its potential application as a remediation source in Fukushima Prefecture, it is also very costly. The ten grams purchased for this initial experimentation cost $1,100. This limits its scaling-up possibilities and requires the discovery of alternatives. These alternative organic ligands should stem from WCA's with a boron base and fluorinated phenyl groups. Once a suite of alternative ligands has been discovered they should be tested alongside TFPB by creating aqueous mixtures of each ligand in the alkali metals and magnesium. Inputting a known quantity of Cs^+, the precipitates can be collected, and the precipitate masses compared to the TFPB precipitate to confirm which alternative would best replace TFPB relative to costs. Testing should then move to a comparison of efficiency to extract radiocesium from Fukushima Prefecture soil.

Conclusions

This thesis took an integrative approach to the radiocesium contamination problem in Fukushima Prefecture. Multiple projects were proposed in the beginning of the research. However, due to insufficient information in the current literature, the first part of this research required the development of a Cs^+ adsorption envelope and the Cs^+ adsorption kinetics to vermiculite. It was observed that as soil pH increased the total adsorbed Cs^+ increased. As soil pH decreases the total adsorbed Cs^+ decreases. Conflicting evidence was presented when observing the Cs^+ adsorption kinetics. The results of this study could definitively agree either opposing arguments on the timing at which the kinetics occur. Using K^+ to initiate interlayer collapse, Cs^+ showed that it can preferentially adsorb to vermiculite interlayers regardless of the time at which K^+-vermiculite interactions occur. This is detrimental to Fukushima Prefecture post-FDNPP accident as it provides evidence suggesting that $^{137}Cs^+$ can access clay interlayers even if they were considered collapsed from previous cation interactions. In fact, it was shown by EXAFS spectroscopy that cesium appeared to be mainly held in the interlayer of clays (Qin *et al.* 2012), supporting the model developed from results found in this study.

The bioindicator research intended to provide an alternative means of monitoring radiocesium movement and evaluate ecological health by showing physiological changes when absorbing radiocesium, which is known to cause cellular and DNA damage. It was suggested that plants can uptake radiocesium through potassium channels and carriers when the plant is in a growing medium depleted of potassium. However, neither plant species chosen for this research showed physiological changes that could be directly correlated to radiocesium uptake. The second part of this research will analyze the plant parts of radiocesium uptake and evaluate their ability to serve as phytoremediation candidates. Results for this portion are currently pending.

A chemical extraction method proposed by Tamura *et al*. 2013 was extended in this research to isolate the clay fraction and remove organic material from contaminated Fukushima Prefecture soil so

that it could be treated with a Cs^+-capturing ligand. Successful extractions were recorded with proposed methods of improvement in the future. The outcome of this research has the potential to greatly impact restoration efforts in Fukushima Prefecture if the costs of the method were to be decreased and the method scaled up to accommodate for larger sample sizes.

The work completed in this thesis is a culmination of two years' work in the Master of Science in Integrative Biology Program at Kennesaw State University. The goal of this research was to provide information that could be used as a baseline for future restoration studies in Fukushima Prefecture.

Literature Cited

(1) **Aliyu AS, Evangeliou N, Mousseau TA, Wu J, Ramli AT.** 2015. An overview of current knowledge concerning the health and environmental consequences of the Fukushima Daiichi Nuclear Power Plant (FDNPP) accident. Environmental International. 85: 213-228.

(2) **Becker D, Dreyer I, Hoth S, Reid JD, Busch H, Lehnen M, Palme K, Hedrich R.** 1996. Changes in voltage activation, Cs^+ sensitivity, and ion permeability in H5 mutants of the plant K^+ channel KAT1. Proceedings of the National Academy of Sciences, USA. 93: 8123-8128.

(3) **Beresford NA.** 2006. Land contaminated by radioactive materials. Soil Use and Management. 21: 468-474.

(4) **Bouzidi A, Souahi F, Hanini S.** 2010. Sorption behavior of cesium on Ain Oussera soil under different physiochemical conditions. Journal of Hazardous Materials. 184: 640-646.

(5) **Brady NC, Weil RR.** 2008. The Nature and Properties of Soils. Pearson Prentice Hall.

(6) **Brouwer E, Baeyens B, Maes A, Cremers A.** 1983. Cesium and rubidium ion equilibria in illite clay. Journal of Physical Chemistry. 87: 1213-1219.

(7) **Campbell LS, Davies BE.** 1995. Soil sorption of caesium modelled by the Langmuir and Freundlich isotherm equations. Applied Geochemistry. 10: 715-723.

(8) **Carignan V, Villard MA.** 2002. Selecting indicator species to monitor ecological integrity: a review. Environmental Monitoring and Assessment. 78(1): 45-61.

(9) **Carreras L, Rovira L, Vaquero M, Mon I, Martin E, Benet-Buchhloz J, Vidal-Ferran A.** 2017. Syntheses, characterisation and solid-state study of alkali and ammonium BArF salts. RSC Advances. 7(52): 32833-32841.

(10) **Chorover J, Choi S, Rotenberg P, Seme RJ, Rivera N, Strepka C, Thompson A, Muller KT, O'Day PA.** 2008. Silicon control of strontium and cesium partitioning in hydroxide-weathered sediments. Geochimica et Cosmochimica Acta. 72: 2024-2047.

(11)**Cline JF, Hungate FP.** 1960. Accumulation of potassium, caesium and rubidium in bean plants grown in nutrient solutions. Plant Physiology. 35: 826-829.

(12)**Comans RNJ, Haller M, DePreter P**. 1990. Sorption of cesium on illite: Non-equilibrium behavior and reversibility. Geochimica et Cosmochimica Acta. 55: 433-440.

(13)**Comans RNJ, Hockley DE**. 1992. Kinetics of cesium sorption on illite. Geochimica et cosmochimica acta. 56(3): 1157-1164.

(14)**de Koning A, Comans RNJ.** 2004. Reversibility of radiocesium sorption on illite. Geochimica et Cosmochimica Acta. 68: 2815-2823.

(15)**de Koning A, Comans RNJ**. 2015. Reversibility of radiocesium sorption on illite. Geochimica et Cosmochimica Acta. 68: 2815-2823.

(16)**de Koning A, Konoplev AV, Comans RNJ.** 2007. Measuring the specific caesium sorption capacity of soils, sediments and clay minerals. Applied Geochemistry. 22: 291-229.

(17)**Dyer A, Chow JKK, Umar IM.** 2000. The uptake of caesium and strontium radioisotopes onto clays. Journal of Materials Chemistry. 10: 2734-2740.

(18)**Dzene L, Tertre E, Hubert F, Ferrage E.** 2015. Nature of the sites involved in the process of cesium desorption from vermiculite. Journal of Colloid and Interface Science. 455: 254-260.

(19)**Ferreira DR, Schulthess CP.** 2011. The Nanopore Inner-Sphere Enhancement (NISE) Effect: Sodium, Potassium, and Calcium. Soil Science Society of America Journal. 75 2: 389-396.

(20)**Ferreira DR, Thornhill JA, Ninova EI**. 2018. The Impact of pH and Ion Exchange on 133Cs Adsorption on Vermiculite. Journal of Environmental Quality. Submitted.

(21)**Fuller AJ, Shaw S, Ward MB, Haigh SJ, Mosselmans JFW, Peacock CL, Stackhouse S, Dent AJ, Trivedi D, Burke IT**. 2015. Caesium incorporation and retention in illite interlayers. Applied Clay Science. 108: 128-134.

56

(22) **Gassmann W, Rubio F, Schroeder JI**. 1996. Alkali cations selectivity of the wheat root high-affinity potassium transporter HKT1. The Plant Journal. 10: 869-882.

(23) **Grutter A, Gunten HR, Rosler E.** 1986. Sorption, desorption, and isotope exchange of cesium (10^{-9} – 10^{-3} M) on chlorite. Clays and Clay Minerals. 34: 677-680.

(24) **Holm E.** 1997. Collection and preparation of marine samples for radionuclide analysis. Strategies and Methodologies for Applied Marine Radioactivity Studies. 271-278.

(25) **Holm E, Samualsson C, Holstensson M.** 2006. Concentration factors and aggregated transfer factors in selected bio-indicators from Sweden. NKS-140.

(26) **Huang M, Hieftje G.** 1989. Simultaneous measurement of spatially resolved electron temperatures, electron number densities and gas temperatures by laser light scattering from the ICP. Spectrochimica Acta Part B: Atomic Spectroscopy. 44: 739-749.

(27) **Jacobs DG, Tamura T.** 1960. The mechanism of ion fixation using radio-isotope techniques. In: 7th International Congress of Soil Science. The International Society of Science, Madison, Wisconsin, USA, pp. 206-214.

(28) **Japanese Ministry of the Environment.** 2011. Decontamination Guidelines Ver. 1, Dec. 2011.

(29) **Kagan LM, Kadatsky VB.** 1996. Depth migration of Chernobyl originated ^{137}Cs and ^{90}Sr in soils of Belarus. Journal of Environmental Radioactivity. 33(1): 27-39.

(30) **Kamada N, Saito O, Endo S, Kimura A, Shizuma K.** 2012. Radiation doses among residents living 37 km northwest of the Fukushima Dai-ichi Nuclear Power Plant. Journal of Environmental Radioactivity. 110:84-89.

(31) **Kato H, Onda Y, Teramage M.** 2012. Depth distribution of 137Cs, 134Cs, and 131I in soil profile after Fukushima Dai-ichi Nuclear Power Plant Accident. Journal of Environmental Radioactivity. 111: 59-64.

(32) **Kobayashi D, Okouchi T, Yamagami M, Shinano T.** 2014. Verification of radiocesium decontamination from farmlands by plants if Fukushima. Journal of Plant Research. 127: 51-56.

(33) **Kozubov GM, Taskaev AI.** 2007. Characteristics of morphogenesis and growth processes of conifers in the Chernobyl nuclear accident zone. Radiatsionnaia Biologiia, Radioecologia. 47: 204-223.

(34) **Lamseejan S, Jompuk P, Wongpiyasatid A, Deeseepan S, Kwanthammachart P.** 2000. Gamma-rays Induced Morphological Changes in Chrysanthemum (Chrysanthemum morifolium). Kasetsart J. (Nat. Sci.). 34(3): 417-422.

(35) **Krauskopf KB, Bird DK.** 1995. Introduction to Geochemistry, third ed. McGraw-Hill, New York.

(36) **Maathuis FJM, Sanders D.** 1994. Mechanism of high-affinity potassium uptake in roots *Arabidopsis thaliana*. Proceedings of the National Academy of Science, USA. 91(20): 9272-9276.

(37) **Maathuis FJM, Sanders D.** 1997. Regulation of K^+ absorption in plant root cells by external K^+: interplay of different plasma membrane K^+ transporters. Journal of Experimental Botany. 48: 451-458.

(38) **Maekawa A, Momoshima N, Sugihara S, Ohzawa R, Nakama A.** 2015. Analysis of 134Cs and 137Cs distribution in soil of Fukushima prefecture and their specific adsorption on clay minerals. Journal of Radioanalytical and Nuclear Chemistry. 303: 1485-1489.

(39) **Menzel RG, Heald WR.** 1955. Distribution of potassium, rubidium, cesium, calcium, and strontium within plants grown in nutrient solutions. Soil Science. 78: 287-293.

(40) **Mukai H, Motai S, Yaita T, Kogure T.** 2016. Identification of the actual cesium-adsorbing materials in the contaminated Fukushima soil. Applied Clay Science. 121-122: 188-193.

(41) **Murota K, Saito T, Tanaka S.** 2016. Desorption kinetics of cesium from Fukushima soils. Journal of Environmental Radioactivity. 153: 134-140.

(42) **Nishida H, Takada N, Yoshimura M, Sonoda T, Kobayashi H.** 1984. Tetrakis [3, 5-bis (trifluoromethyl) phenyl] borate. Highly lipophilic stable anionic agent for solvent-extraction of cations. Bulletin of the Chemical Society of Japan. 57(9): 2600-2604.

(43) **Nishita H, Dixon D, Larson KH.** 1962. Accumulation of Cs and K and growth of bean plants in nutrient solution and soils. Plant and Soil. 17: 221-242.

(44) **Nissen P.** 1991. Uptake mechanisms. In: Waisel Y, Eshel A, Kafkafi U, eds. Plant roots: the hidden half. USA: Marcel Dekker Inc.

(45) **Ohba K.** 1964. Studies on radiosensitivity and induction of somatic mutations in forest trees. Gamma Field Symposia (Japan). 3.

(46) **Qin H, Yokoyama Y, Fan Q, Iwatani H, Tanaka K, Sakaguchi A, Kanai Y, Zhu J, Onda Y, Takahashi Y.** 2012. Investigation of cesium adsorption on soil and sediment samples from Fukushima Prefecture by sequential extraction and EXAFS technique. Geochemical Society of Japan. 46(4): 297-302.

(47) **Rani RD, Sasidhar P.** 2012. Sorption of Cesium on Clay Colloids: Kinetic and Thermodynamic Studies. Aquatic Geochemistry. 18: 281-296.

(48) **Sano O, Ito T, Ando T, Nanzyo M, Saito G, Saigusa M.** 2010. Clay mineralogical composition of representative paddy soils in southern part of northeastern Japan. Japanese Society of Pedology. 54(2): 83-92.

(49) **Sawhney BL.** 1964. Sorption and Fixation of Microquantities of Cesium by Clay Minerals: Effect of Saturating Cations. Soil Science Society of America Journal. 28(2): 183-186.

(50) **Sawhney BL.** 1972. Selective sorption and fixation of cations by clay minerals: a review. Clays and Clay Minerals. 20: 93-100.

(51) **Schachtman DP, Schroeder JI, Lucas WJ, Anderson JA, Gaber RF.** 1992. Expression of an inward rectifying potassium channel by the *Arabidopsis* KAT1 cDNA. Science. 258: 1654-1658.

(52)**Schachtman DP, Schroeder JI.** 1994. Structure and transport mechanism of a high-affinity potassium uptake transporter from higher plants. Nature. 370: 655-658.

(53)**Shaw G, Bell JNB.** 1991. Competitive effects of potassium and ammonium on caesium uptake kinetics in wheat. Journal of Environmental Radioactivity. 13: 283-296.

(54)**Shaw G, Hewamanna R, Lillywhite J, Bell JNB.** 1992. Radiocaesium uptake and translocation in wheat with reference to the transfer factor concept and ion competition effects. Journal of Environmental Radioactivity. 16: 167-180.

(55)**Shiga Clean Water Website.** www.kouka.ne.jp/-skj-ccs/clean/riyo.html#hyou02

(56)**Schulthess CP and Huang CP.** 1990. Adsorption of Heavy Metals by Silicon and Aluminum Oxide Surfaces on Clay Minerals. Soil Science Society of America Journal. 54: 679-688.

(57)**Shcheglov AI, Tsvetnova OB, Stolbova VV.** 2013. Bioindication of Radioactive Contamination of Natural Ecosystems. Moscow University Science Bulletin. 68: 185-191.

(58)**Soil Quality Indicators: Aggregate Stability**. USDA Natural Resources Conservation Service. 1996.

(59)**Sparks DL, Fendorf SE, Toner CV, Carski TH.** 1996. Methods of Soil Analysis: Part 3, Chemical Methods. Soil Science Society of America, Inc., Madison, WI.

(60)**Sparrow AH, Schairer IA, Woodwell GM.** 1965. Tolerance of Pinus rigida trees to a ten-years exposure to chronic gamma irradiation from cobalt-60. Radiation Botany. 5: 7-22.

(61)**Sparrow AH, Woodwell GM.** 1962. Prediction of the sensitivity of plants to chronic gamma irradiation. Radiation Botany. 2: 9-12.

(62)**Tamura K, Sato H, Yamagishi A.** 2015. Desorption of Cs^+ ions from a vermiculite by exchanging Mg^{2+} ions: effects of Cs^+-capturing ligand. Journal of Radioanalytical and Nuclear Chemistry. 303(3): 2205-2210.

(63)**Tanaka K, Managi S.** 2016. Impact of a disaster on land price: evidence from Fukushima nuclear power plant accident. The Singapore Economic Review 61: 15 pages.

(64) **"The 2007 Recommendations of the International Commission on Radiological Protection."** Annals of the ICRP. ICRP Publication. 103. 37(2-4). 2007.

(65) **Wang TB, Gassmann W, Rubio F, Schroeder JI, Glass ADM**. 1998. Rapid up-regulation of HKT1, a high-affinity potassium transporter gene, in roots of barley and wheat following withdrawal of potassium. Plant Physiology. 118: 651-659.

(66) **Ward J**. 2014. DNA damage produced by ionizing radiation in mammalian cells: identities, mechanisms of formation, and reparability. Progress in nucleic research and molecular biology. Academic Press. 35: 95-125.

(67) **Watanabe Y, Ichikawa S, Kubota M, Hoshino J, Kubota Y, Maruyama K, Fuma S, Kawaguchi I, Yoschenko V, Yoshida S.** 2015. Morphological defects in native Japanese fir trees around the Fukushima Daiichi Nuclear Power Plant. Scientific Reports. DOI: 10.1038/srep13232.

(68) **Wi S, Chung BY, Kim JS, Kim JH, Baek MH, Lee JW, Kim YS.** 2007. Effects of gamma irradiation on morphological changes and biological responses in plants. Micron. 38: 553-564.

(69) **Yasunari TJ, Stohl A, Hayano RS, Burkhart JF, Eckhardt S, Yasunari T.** 2011. Cesium-137 deposition and contamination of Japanese soils due to the Fukushima nuclear accident. Proceedings of the National Academy of Sciences, USA. 108: 19530-19534.

(70) **Yasutaka T, Naito W.** 2016. Assessing the cost and effectiveness of radiation decontamination in Fukushima Prefecture. Journal of Environmental Radioactivity. 151: 512-520.

(71) **Zhu YG, Shaw G, Nisbet AF, Wilkins BT.** 2000. Effect of potassium starvation on the uptake of radiocesium by spring wheat (*Triticum aestivum* cv. Tonic). Plant and Soil. 220: 27-34.

(72) **Zhu YG, Shaw G.** 2000. Soil contamination with radionuclides and potential remediation. Chemosphere 41: 121-128.

Appendix

Cesium Adsorption Envelope Data

JAT-1	Vermiculite		[Cs]
Sample ID	(g)	pH	(mM)
1	1.0006	12.43	6.13
2	1.0002	6.96	8.31
3	1.0007	2.63	10.14
4	1.0008	1.51	12.62
5	0.9994	1.04	13.71
6	0.9993	0.82	14.52

JAT-2	Vermiculite		[Cs]
Sample ID	(g)	pH	(mM)
1	0.9996	12.08	6.43
2	0.9995	10.05	7.56
3	1.0009	9.30	7.90
4	1.0003	8.05	8.09
5	1.0007	4.94	9.50
6	1.0005	3.32	10.35
7	1.0007	3.19	10.28
8	0.9998	1.58	12.06

JAT-9	Vermiculite		[Cs]
Sample ID	(g)	pH	(mM)
1	0.9998	7.87	7.59
2	0.9990	8.39	8.16
3	1.0010	7.87	8.27
4	1.0010	7.10	8.64
5	1.0008	5.91	9.18
6	1.0007	4.79	10.44
7	0.9999	4.32	11.79
8	0.9991	3.78	12.35
9	1.0006	3.53	13.23
10	1.0008	3.00	13.12
11	0.9996	3.06	12.99
12	1.0003	3.04	12.89
13	1.0009	2.93	13.11
14	1.0010	3.09	13.13
15	1.0005	2.91	13.36
16	0.9992	2.89	13.08
17	1.0005	2.97	13.21
18	1.0009	2.74	13.42
19	0.9992	2.69	13.45
20	1.0007	2.01	14.35

JAT-10 Sample ID	Vermiculite (g)	pH	[Cs] (mM)
1	1.0024	7.19	7.95
2	1.0006	6.96	8.12
3	1.0003	5.18	8.93
4	1.0018	4.80	9.30
5	1.0016	5.54	9.31
6	1.0002	4.29	10.53
7	1.0029	3.24	12.96
8	1.0024	1.74	14.46
9	0.9997	1.47	15.16
10	1.0023	1.33	15.42
11	0.9992	1.19	15.16
12	0.9994	1.07	15.61
13	1.0029	1.04	15.51
14	0.9998	0.98	15.41
15	1.0014	0.95	15.37
16	1.0026	5.08	8.89

JAT-14 Sample ID	Vermiculite (g)	pH	[Cs] (mM)
1	0.0000	12.79	40.33
2	1.0013	4.68	25.45
3	1.0007	2.09	31.44
4	1.0017	1.71	31.64
5	0.9997	1.48	32.45
6	0.9990	1.37	32.57
7	1.0004	1.25	32.35
8	0.9998	1.15	32.37
9	1.0011	1.06	32.06
10	1.0023	1.00	32.61
11	1.0018	0.96	33.36
12	1.0025	0.73	34.31
13	1.0003	0.52	34.89
14	1.0007	0.44	34.17
15	1.0011	0.38	33.73
16	1.0000	0.26	35.27

JAT-15	Vermiculite		[Cs]
Sample ID	(g)	pH	(mM)
1	0.9990	9.78	20.13
2	1.0000	9.99	19.55
3	1.0023	9.95	19.96
4	1.0023	9.74	20.10
5	1.0024	9.66	20.89
6	1.0025	9.59	20.32
7	0.9986	9.38	21.56
8	1.0016	9.48	20.77
9	1.0017	9.18	21.47
10	0.9986	9.29	21.33
11	0.9990	8.99	22.64
12	1.0023	8.94	22.74
13	1.0014	8.79	22.92
14	1.0000	8.72	22.59
15	1.0013	8.90	22.95
16	1.0028	8.54	24.07

JAT-20	Vermiculite		[Cs] final
Sample ID	(g)	pH	mM
BLK	0.0000	12.64	41.02
1	0.9990	9.74	20.02
2	1.0025	9.12	21.45
3	1.0010	8.28	23.90
4	1.0003	8.69	23.48
5	0.9982	8.45	23.71
6	1.0012	7.87	24.03
7	1.0023	7.71	23.95
8	0.9992	7.94	23.78
9	0.9985	6.26	25.73
10	1.0019	5.22	26.01
11	1.0008	4.29	27.80
12	0.9996	3.88	28.19
13	1.0024	3.55	29.71
14	1.0019	3.34	30.42
15	1.0017	2.59	29.31
16	1.0018	2.28	27.92

JAT-21	Vermiculite		[Cs] final
Sample ID	(g)	pH	mM
1	0.9991	9.28	22.19
2	0.9998	8.96	22.76
3	1.0002	8.71	23.11
4	0.9999	8.50	22.89
5	1.0006	8.23	23.35
6	0.9990	8.22	23.55
7	0.9995	8.05	23.76
8	1.0017	7.74	23.96
9	1.0015	4.73	25.25
10	1.0005	3.46	27.12
11	0.9993	2.68	27.27
12	1.0017	1.32	-9.50
13	1.0018	1.21	-25.21
14	0.9993	1.02	-27.92
15	0.9992	1.09	-34.33
16	1.0015	0.54	-190.12

JAT-27	Vermiculite		[Cs]
Sample ID	(g)	pH	mM
10 (BLK)	0.9996	12.20	20.11
1	1.0015	2.62	23.50
2	0.9982	2.22	21.57
3	0.9989	3.42	26.00
4	1.0005	2.91	25.37
5	1.0000	2.38	23.10
6	1.0019	7.45	23.75
7	0.9997	6.24	23.83
8	0.9987	7.50	23.05
9	1.0014	8.17	23.15
27-1	0.9996	6.35	23.15
27-1	1.0014	5.02	23.34

JAT-27	Vermiculite		[Cs]
Sample ID	(g)	pH	ppm
1	0.9995	11.76	2807.14
2	0.9983	11.59	2824.83
3	1.0002	3.49	3710.03
4	0.9993	2.84	3715.51
5	1.0009	2.67	3743.77
6	1.0006	2.42	3769.53
7	0.9983	2.34	3756.11
8	0.9988	1.42	2970.37
9	1.0003	1.31	2491.49
10	1.0006	0.74	N/A
BLANK	0.0000	13.16	5507.36

JAT-27	Vermiculite		[Cs]
Sample ID	(g)	pH	ppm
DIL-1	0.9995	11.76	259.35
DIL-2	0.9983	11.59	284.03
DIL-3	1.0002	3.49	339.47
DIL-4	0.9993	2.84	334.80
DIL-5	1.0009	2.67	373.21
DIL-6	1.0006	2.42	393.83
DIL-7	0.9983	2.34	370.81
DIL-8	0.9988	1.42	313.88
DIL-9	1.0003	1.31	249.94
DIL-10	1.0006	0.74	N/A

JAT-27	Vermiculite		[Cs]
Sample ID	(g)	pH	ppm
1-FIL	0.9988	9.66	2703.46
2-FIL	0.9988	9.68	2826.24
3-FIL	1.0000	8.93	2912.97
4-FIL	0.9992	8.06	3117.70
5-FIL	1.0008	7.79	3045.41
6-FIL	0.9998	5.28	3318.69
7-FIL	0.9988	3.99	3492.49
8-FIL	1.0018	3.35	3515.34
9-FIL	0.9983	2.55	3433.83
10-FIL	0.9984	0.73	N/A
BLANK	0	12.43	5094.48
6-DIL	0.9998	5.28	3227.00
7-DIL	0.9988	3.99	2673.30
8-DIL	1.0018	3.35	2334.00
9-DIL	0.9983	2.55	2823.80
10-DIL	0.9984	0.73	N/A

JAT-28	Vermiculite		[Cs]
Sample ID	(g)	(pH)	(ppm)
1	0.9995	11.76	2807.14
2	0.9983	11.59	2824.83
3	1.0002	3.49	3710.03
4	0.9993	2.84	3715.51
5	1.0009	2.67	3743.77
6	1.0006	2.42	3769.53
7	0.9983	2.34	3756.11
8	0.9988	1.42	2970.37
9	1.0003	1.31	2491.49
10	1.0006	0.74	N/A
BLANK	0.0000	13.16	5507.36

JAT-28	Vermiculite		[Cs]
Sample ID	(g)	(pH)	ppm
DIL-1	0.9995	11.76	2593.50
DIL-2	0.9983	11.59	2840.30
DIL-3	1.0002	3.49	3394.70
DIL-4	0.9993	2.84	3348.00
DIL-5	1.0009	2.67	3732.10
DIL-6	1.0006	2.42	3938.30
DIL-7	0.9983	2.34	3708.10
DIL-8	0.9988	1.42	3138.80
DIL-9	1.0003	1.31	2499.40
DIL-10	1.0006	0.74	N/A

JAT-29	Vermiculite		[Cs]
Sample ID	(g)	pH	ppm
1-FIL	0.9988	9.66	2703.46
2-FIL	0.9988	9.68	2826.24
3-FIL	1.0000	8.93	2912.97
4-FIL	0.9992	8.06	3117.70
5-FIL	1.0008	7.79	3045.41
6-FIL	0.9998	5.28	3318.69
7-FIL	0.9988	3.99	3492.49
8-FIL	1.0018	3.35	3515.34
9-FIL	0.9983	2.55	3433.83
10-FIL	0.9984	0.73	N/A
BLANK	0	12.43	5094.48
6-DIL	0.9998	5.28	3227.00
7-DIL	0.9988	3.99	2673.30
8-DIL	1.0018	3.35	2334.00
9-DIL	0.9983	2.55	2823.80
10-DIL	0.9984	0.73	N/A

JAT-31	Vermiculite		[Cs]
Sample ID	(g)	pH	ppm
2	0.9999	9.51	2927.38
3	1.0015	8.86	3096.19
4	1.0007	7.92	3155.06
5	0.9996	7.52	3133.39
6	1.0003	4.40	3371.9
7	1.0009	3.66	3459.73
8	0.9991	2.86	3528.26
9	1.0023	2.38	3559.72
10	1.0024	0.52	3512.39
BLANK	0.0000	13.35	5049.82
FIL-1	1.0026	N/A	2645.4
FIL-2	0.9999	N/A	2898.82
FIL-3	1.0015	N/A	3049.29
FIL-4	1.0007	N/A	3149.05
FIL-5	0.9996	N/A	3165.48
FIL-6	1.0003	N/A	3449.81
FIL-7	1.0009	N/A	3557.6
FIL-8	0.9991	N/A	3555.06
FIL-9	1.0023	N/A	3510.51
FIL-10	1.0024	N/A	3529.15
FIL-BLK	0.0000	N/A	5070.12

JAT-32	Vermiculite		[Cs]
Sample ID	(g)	pH	ppm
1	1.0022	8.54	3205.07
2	1.0013	8.39	3179.29
3	0.9997	7.94	3234.6
4	1.0002	7.42	3220.61
5	1.0013	7.06	3208.03
6	1.0001	6.75	3201.53
7	1.0002	5.28	3355.74
8	1.0007	5.09	3330.16
9	0.9987	4.80	3375.46
10	0.9998	4.80	3379.72
11	1.0009	4.53	3467.18
12	1.0011	3.86	3591.83
13	1.0004	2.51	3659.12
14	0.9984	1.60	3869.19
15	0.9994	1.01	3902.97
16	1.0004	0.80	3813.53
BLANK	0.0000	12.68	5244.11
FIL-1	1.0022	8.54	3194.25
FIL-2	1.0013	8.39	3216.72
FIL-3	0.9997	7.94	3240.46
FIL-4	1.0002	7.42	3274.72
FIL-5	1.0013	7.06	3283.98
FIL-6	1.0001	6.75	3286.13
FIL-7	1.0002	5.28	3433.54
FIL-8	1.0007	5.09	3386.55
FIL-9	0.9987	4.80	3408.47
FIL-10	0.9998	4.80	3420.83
FIL-11	1.0009	4.53	3503.51
FIL-12	1.0011	3.86	3602.91
FIL-13	1.0004	2.51	3639.71
FIL-14	0.9984	1.60	3861.71
FIL-15	0.9994	1.01	4015.36
FIL-16	1.0004	0.80	3843.86

JAT-33	Vermiculite		[Cs]
Sample ID	(g)	pH	ppm
1	0.9995	9.80	2888.53
2	1.0018	9.81	2861.92
3	1.0002	7.82	3146.15
4	1.0017	6.52	3182.83
5	1.0015	7.07	3147.19
6	1.0023	7.14	3167.32
7	1.0024	6.89	3172.07
8	1.0002	7.00	3186.63
9	1.0018	6.88	3198.3
10	0.9992	7.03	3176.5
11	1.0021	6.17	3191.36
12	1.0023	6.68	3135.78
13	0.9994	6.51	3125.81
14	0.9998	6.79	3147.41
15	0.9999	3.75	3527.76
16	1.0003	3.96	3517.29
BLANK	0.0000	12.86	5059.16
FIL-1	0.9995	9.80	2875.37
FIL-2	1.0018	9.81	2847.06
FIL-3	1.0002	7.82	3133.8
FIL-4	1.0017	6.52	3176.21
FIL-5	1.0015	7.07	3111.73
FIL-6	1.0023	7.14	3203.91
FIL-7	1.0024	6.89	3128.24
FIL-8	1.0002	7.00	3181.03
FIL-9	1.0018	6.88	3211.39
FIL-10	0.9992	7.03	3170.12
FIL-11	1.0021	6.17	3133.25
FIL-12	1.0023	6.68	3170.5
FIL-13	0.9994	6.51	3137.02
FIL-14	0.9998	6.79	3180.65
FIL-15	0.9999	3.75	3464.27
FIL-16	1.0003	3.96	3437.79

JAT-34	Vermiculite		[Cs]
Sample ID	(g)	pH	ppm
1	0.9998	6.00	3498.73
2	1.0010	5.51	3528.8
3	1.0021	5.95	3558.26
4	1.0008	5.72	3453.98
5	1.0002	5.51	3565.93
6	1.0012	5.71	3468.17
BLANK	0.0000	12.72	5515.79
FIL-1	0.9998	6.00	3476.77
FIL-2	1.0010	5.51	3586.94
FIL-3	1.0021	5.95	3495.47
FIL-4	1.0008	5.72	3550.58
FIL-5	1.0002	5.51	3557.42
FIL-6	1.0012	5.71	3538.27

JAT-35	Vermiculite		[Cs]
Sample ID	(g)	pH	ppm
1	1.0000	2.31	3919.35
2	0.9984	2.24	4006.23
3	0.9994	1.99	4101.50
4	1.0024	1.73	4028.29
5	1.0020	1.69	4096.59
BLANK	0.0000	13.23	5563.28
FIL-1	1.0000	2.31	3945.54
FIL-2	0.9984	2.24	4028.38
FIL-3	0.9994	1.99	4072.50
FIL-4	1.0024	1.73	4143.92
FIL-5	1.0020	1.69	4195.87

Cesium Adsorption Kinetics Data

JAT-59	Adsorption Kinetics - 2.5 min KOH Addition		
Sample ID	Solids (g)	pH	[Cs+] ppm
1	0.9993	12.48	3507.88
2	0.9997	11.81	3394.86
3	1.0011	11.05	3288.57
4	1.0019	10.18	3316.46
5	1.0011	9.64	3364.82
6	1.0026	8.80	3470.04
7	1.0027	8.49	3670.91
8	1.0002	7.96	3592.54
9	1.0026	7.28	3695.27
10	0.9999	6.66	3855.35
11	1.0015	4.46	3965.74
12	1.0022	3.09	4079.47
13	0.9990	2.60	4010.91
14	1.0012	1.95	4057.92
15	1.0012	1.66	4162.50
BLK	0.0000	13.10	5602.87

JAT-59	Adsorption Kinetics - 2.5 min KOH Addition		
Sample ID	Solids (g)	pH	[Cs+] ppm
1	0.9993	10.77	3372.50
2	0.9999	5.85	3496.34
3	0.9994	5.44	3526.84
4	1.0016	4.99	3653.13
5	1.0015	4.35	3656.13
6	0.9982	4.14	3701.28
7	0.9997	3.56	3835.64
8	1.0010	1.60	3876.32
9	0.9995	1.53	4203.66
10	1.0010	1.46	4219.60
BLK	0.0000	13.04	5206.31

JAT-48	Adsorption Kinetics - 5 min KOH Addition		
Sample ID	Solids (g)	pH	[Cs+] ppm
1	0.9993	9.67	2238.65
2	1.0018	9.35	2156.52
3	1.0021	8.75	2286.37
4	1.0027	8.33	2274.88
5	1.0026	7.06	2399.88
6	1.0013	6.36	2316.60
7	1.0026	5.13	2302.86
8	1.0029	4.34	2465.09
9	1.0011	3.94	2478.52
10	1.0011	3.68	2457.00
BLK	0.0000	12.94	5337.81

JAT-56	Adsorption Kinetics - 10 min KOH Addition		
Sample ID	Solids (g)	pH	[Cs+] ppm
1	1.0015	12.73	3025.75
2	1.0013	11.21	2328.57
3	1.0006	11.51	3041.37
4	0.9989	10.71	3218.67
5	1.0017	10.20	3166.48
6	1.0013	8.36	2287.14
7	1.0020	8.95	2999.20
8	1.0028	8.54	2985.36
9	0.9989	8.00	3117.26
10	1.0005	7.33	3047.26
11	0.9991	5.10	3305.21
12	1.0006	3.92	3502.48
13	0.9995	3.50	3433.29
14	1.0008	2.86	3415.43
15	1.0011	2.60	3547.23
BLK	0.0000	13.36	4613.96

JAT-57	Adsorption Kinetics - 10 min KOH Addition		
Sample ID	Solids (g)	pH	[Cs+] ppm
1	1.0021	8.69	3131.18
2	1.0015	8.81	2969.26
3	1.0019	5.97	3089.95
4	1.0024	5.82	3031.37
5	1.0026	5.44	3056.16
6	1.0021	4.90	3130.25
7	1.0018	1.72	3492.29
8	1.0006	1.62	3537.77
9	1.0005	1.49	3546.64
10	0.9997	1.43	3644.68
BLK	0.0000	13.11	4501.17

JAT-62	Adsorption Kinetics - 0 min KOH Addition		
Sample ID	Solids (g)	pH	[Cs+] ppm
1	1.0013	6.26	3267.81
2	0.9998	6.44	3379.50
3	1.0020	6.22	3371.00
4	1.0013	4.63	3504.54
5	0.9982	4.19	3590.82
6	1.0007	3.64	3609.82
7	0.9989	2.03	3674.70
8	1.0004	1.86	3636.96
9	1.0014	1.74	3769.46
BLK	0.0000	12.98	5075.14

JAT-62	Adsorption Kinetics - 2.5 min KOH Addition		
Sample ID	Solids (g)	pH	[Cs+] ppm
1	0.9998	6.51	3281.96
2	0.9996	6.37	3324.18
3	0.9988	6.07	3290.73
4	1.0007	4.65	3437.40
5	1.0019	4.29	3523.70
6	0.9983	3.71	3632.52
7	0.9989	2.07	3756.50
8	1.0003	1.86	3758.09
9	0.9987	1.70	3828.18
BLK	0.0000	12.98	5075.14

JAT-62	Adsorption Kinetics - 5 min KOH Addition		
Sample ID	Solids (g)	pH	[Cs+] ppm
1	1.0001	6.63	3403.69
2	1.0001	6.43	3356.40
3	1.0027	6.29	3402.71
4	0.9993	4.93	3493.71
5	0.9997	4.44	3642.23
6	0.9987	3.83	3684.75
7	1.0015	2.10	3728.15
8	1.0022	1.93	3793.98
9	0.9983	1.80	3725.66
BLK	0.0000	12.98	5075.14

JAT-64	Adsorption Kinetics - 24 hour CsOH Addition			
Sample ID	Solids (g)	pH	[Cs+] ppm	[K+] ppm
1	0.9985	7.41	4269.53	1159.10
2	0.9988	8.38	4311.47	1175.80
3	1.0002	8.71	4350.17	1160.10
4	1.0008	8.48	4258.68	1174.20
5	0.9984	8.21	4294.39	1202.00
6	1.0009	6.90	4309.13	1174.50
7	1.0008	6.71	4338.08	1193.00
8	0.9990	6.80	4360.34	1208.40
9	1.0014	6.60	4566.58	1231.50
BLK	0.0000	13.17	5591.93	1194.70

JAT-65	Adsorption Kinetics -1 hour CsOH Addition			
Sample ID	Solids (g)	pH	[Cs+] ppm	[K+] ppm
1	1.0015	6.79	3288.61	1210.50
2	0.9996	6.71	3293.74	1216.40
3	1.0008	6.59	3272.25	1220.20
4	1.0027	6.51	3311.51	1209.10
5	0.9994	6.44	3219.11	1193.90
6	0.9998	6.33	3236.60	1171.50
7	1.0001	6.11	3249.59	1182.60
BLK	0.0000	12.90	5385.25	1262.80

JAT-65	Adsorption Kinetics - 3 hour CsOH Addition			
Sample ID	Solids (g)	pH	[Cs+] ppm	[K+] ppm
1	1.0022	6.52	3118.61	1163.10
2	1.0020	6.57	3090.09	1140.60
3	1.0012	6.56	3165.14	1164.00
4	1.0011	6.60	3160.43	1166.30
5	0.9996	6.50	3213.26	1165.60
6	1.0017	6.35	3155.33	1152.80
7	1.0009	6.25	3238.50	1166.00
BLK	0.0000	12.90	5385.25	1262.80

JAT-65	Adsorption Kinetics - 36 hour CsOH Addition			
Sample ID	Solids (g)	pH	[Cs+] ppm	[K+] ppm
1	1.0021	7.07	3346.27	1125.30
2	1.0005	6.95	3284.83	1126.50
3	1.0021	7.17	3272.33	1144.90
4	1.0019	6.86	3307.92	1116.90
5	1.0008	6.72	3309.57	1132.70
6	0.9986	6.53	3291.71	1121.00
7	0.9994	6.18	3452.76	1124.50
BLK	0.0000	12.90	5385.25	1262.80

JAT-65	Adsorption Kinetics - 48 hour CsOH Addition			
Sample ID	Solids (g)	pH	[Cs+] ppm	[K+] ppm
1	0.9991	6.97	3206.66	1108.10
2	1.0008	7.33	3256.99	1134.60
3	1.0000	7.20	3324.24	1111.10
4	1.0005	6.98	3309.43	1137.30
5	0.9991	6.90	3347.84	1125.60
6	1.0009	6.58	3269.80	1128.70
7	1.0016	6.54	3361.57	1116.40
BLK	0.0000	12.90	5385.25	1262.80

SS-48	Adsorption Kinetics -12 hour CsOH Addition			
Sample ID	Solids (g)	pH	[Cs+] ppm	[K+] ppm
1	1.0008	7.67	3439.05	1243.73
2	1.0005	7.65	3138.29	1559.42
3	1.0001	7.71	3338.18	1499.35
4	1.0018	7.52	3399.51	1569.27
BLK	0.0000	13.24	5160.24	1563.93

SS-48	Adsorption Kinetics -24 hour CsOH Addition			
Sample ID	Solids (g)	pH	[Cs+] ppm	[K+] ppm
1	1.0018	7.69	3289.22	1485.68
2	1.0024	7.63	3511.60	1504.08
3	1.0011	7.80	3318.21	1591.24
4	1.0003	7.82	3414.34	1463.50
BLK	0.0000	13.24	5160.24	1563.93

SS-48	Adsorption Kinetics -48 hour CsOH Addition			
Sample ID	Solids (g)	pH	[Cs+] ppm	[K+] ppm
1	1.0014	7.96	3684.79	1525.40
2	1.0021	7.89	3289.15	1479.94
3	1.0006	7.88	3538.38	1610.47
4	1.0007	7.89	3457.64	1548.15
BLK	0.0000	13.24	5160.24	1563.93

SS-48	Adsorption Kinetics – 168 hour CsOH Addition			
Sample ID	Solids (g)	pH	[Cs+] ppm	[K+] ppm
1	0.9994	7.84	3596.72	1231.36
2	0.9994	7.70	3484.63	1166.74
3	0.9999	7.79	3405.26	1253.69
4	1.0007	7.48	3557.37	1563.93
BLK	0.0000	13.24	5160.24	1228.73

SS-48	Adsorption Kinetics – 336 hour CsOH Addition			
Sample ID	Solids (g)	pH	[Cs+] ppm	[K+] ppm
1	1.0024	8.08	3540.39	1161.33
2	1.0000	8.02	3644.75	1158.72
3	1.0022	7.59	3762.82	1256.85
4	0.9996	7.86	3433.48	1242.46
BLK	0.0000	13.24	5160.24	1563.93

SS-48	Adsorption Kinetics – 720 hour CsOH Addition			
Sample ID	Solids (g)	pH	[Cs+] ppm	[K+] ppm
1	1.0000	7.94	3903.18	1189.03
2	1.0008	7.61	3661.66	1225.36
3	0.9990	7.46	3173.99	1144.73
4	1.0005	7.52	3739.07	1235.95
BLK	0.0000	13.24	5160.24	1563.93

SS-48	Adsorption Kinetics – 1440 hour CsOH Addition			
Sample ID	Solids (g)	pH	[Cs+] ppm	[K+] ppm
1	1.0017	7.32	3594.30	1189.19
2	1.0008	7.31	3568.92	1163.10
3	0.9993	7.21	3573.53	1157.30
4	0.9997	6.90	3688.25	1183.60
BLK	0.0000	13.24	5160.24	1563.93

Chemical Extraction Data
Trial #1

TREATED SOIL #1		①-Cs134	①-Cs137	②-Cs134	②-Cs137	③-Cs134	③-Cs137
Cs							
decay rate		231	1711	231	1711	231	1711
count(sample)	Gross	404	2297	437	2203	412	2305
weight(sample)	g	0.382	0.382	0.382	0.382	0.382	0.382
count(STD)	Gross	42	103	42	103	42	103
weight(STD)	g	0.558	0.558	0.558	0.558	0.558	0.558
count(Blank)	Gross	25	67	25	67	25	67
radiation	Bq/kg	7523	154819	8178	148293	7681	155374
total	Bq/kg	162341		156470		163056	

TREATED SOIL #2		①-Cs134	①-Cs137
Cs			
decay rate		227	1709
count(sample)	Gross	4781	25968
weight(sample)	g	0.245	0.245
count(STD)	Gross	4989	24474
weight(STD)	g	0.558	0.558
count(Blank)	Gross	366	647
radiation	Bq/kg	493.74	4136.39
total	Bq/kg	4630.13	

TREATED SOIL #3		①-Cs134	①-Cs137
Cs			
decay rate		227	1709
count(sample)	Gross	3404	17391
weight(sample)	g	0.325	0.325
count(STD)	Gross	4989	24474
weight(STD)	g	0.558	0.558
count(Blank)	Gross	366	647
radiation	Bq/kg	256.12	2061.97
total	Bq/kg	2318.09	

TREATED SOIL #4		①-Cs134	①-Cs137
Cs			
decay rate		230	1710
count(sample)	Gross	2993	15302
weight(sample)	g	0.333	0.333
count(STD)	Gross	474	1345
weight(STD)	g	0.558	0.558
count(Blank)	Gross	366	647
radiation	Bq/kg	9374.63	60161.20
total	Bq/kg	69535.83	

UNTREATED SOIL #1		①-Cs134	①-Cs137	②-Cs134	②-Cs137	③-Cs134	③-Cs137
Cs							
decay rate		227	1517	227	1517	227	1517
count(sample)	Gross	3094	17350	2997	17063	2944	17309
weight(sample)	g	2.95	2.95	2.95	2.95	2.95	2.95
count(STD)	Gross	55	132	55	132	55	132
weight(STD)	g	0.558	0.558	0.558	0.558	0.558	0.558
count(Blank)	Gross	40	70	40	70	40	70
radiation	Bq/kg	8742	79974	8464	78646	8313	79784
total	Bq/kg	88716		87110		88097	

UNTREATED SOIL #2		①-Cs134	①-Cs137	②-Cs134	②-Cs137	③-Cs134	③-Cs137
Cs							
decay rate		227	1517	227	1517	227	1517
count(sample)	Gross	2250	12904	2350	12779	2250	12748
weight(sample)	g	1.994	1.994	1.994	1.994	1.994	1.994
count(STD)	Gross	55	132	55	132	55	132
weight(STD)	g	0.558	0.558	0.558	0.558	0.558	0.558
count(Blank)	Gross	40	70	40	70	40	70
radiation	Bq/kg	9359	87875	9783	87019	9359	86807
total	Bq/kg	97234		96802		96166	

UNTREATED SOIL #3		①-Cs134	①-Cs137	②-Cs134	②-Cs137	③-Cs134	③-Cs137
Cs		①-Cs134	①-Cs137	②-Cs134	②-Cs137	③-Cs134	③-Cs137
decay rate		227	1518	227	1518	227	1518
count(sample)	Gross	3043	17312	3025	17563	3025	17767
weight(sample)	g	3.583	3.583	3.583	3.583	3.583	3.583
count(STD)	Gross	48	127	48	127	48	127
weight(STD)	g	0.558	0.558	0.558	0.558	0.558	0.558
count(Blank)	Gross	28	48	28	48	28	48
radiation	Bq/kg	5329	51662	5297	52413	5297	53024
total	Bq/kg	56992		57711		58321	

UTNREATED SOIL #4		①-Cs134	①-Cs137	②-Cs134	②-Cs137
Cs		①-Cs134	①-Cs137	②-Cs134	②-Cs137
decay rate		232	1711	232	1711
count(sample)	Gross	3745	20200	3676	20021
weight(sample)	g	5.235	5.235	5.235	5.235
count(STD)	Gross	129	491	129	491
weight(STD)	g	4	4	4	4
count(Blank)	Gross	41	69	41	69
radiation	Bq/kg	7461	62366	7322	61811
total	Bq/kg	69827		69134	

83

Trial #2

TREATED SOIL #1			
Cs		①-Cs134	①-Cs137
decay rate		217	1704
count(sample)	Gross	3517	19342
weight(sample)	g	0.517	0.517
count(STD)	Gross	451	1307
weight(STD)	g	0.558	0.558
count(Blank)	Gross	398	709
radiation	Bq/kg	13783	57305
total	Bq/kg	71088	

TREATED SOIL #2			
Cs		①-Cs134	①-Cs137
decay rate		217	1704
count(sample)	Gross	3384	18441
weight(sample)	g	0.474	0.474
count(STD)	Gross	451	1307
weight(STD)	g	0.558	0.558
count(Blank)	Gross	398	709
radiation	Bq/kg	14392	59482
total	Bq/kg	73874	

TREATED SOIL #3			
Cs		①-Cs134	①-Cs137
decay rate		217	1704
count(sample)	Gross	4477	24613
weight(sample)	g	0.578	0.578
count(STD)	Gross	451	1307
weight(STD)	g	0.558	0.558
count(Blank)	Gross	398	709
radiation	Bq/kg	16123	65758
total	Bq/kg	81880	

TREATED SOIL #4			
Cs		①-Cs134	①-Cs137
decay rate		218	1704
count(sample)	Gross	3253	16628
weight(sample)	g	0.478	0.478
count(STD)	Gross	528	1316
weight(STD)	g	0.558	0.558
count(Blank)	Gross	364	710
radiation	Bq/kg	4483	52251
total	Bq/kg	56734	

UTNREATED SOIL #1							
Cs		①-Cs134	①-Cs137	②-Cs134	②-Cs137	③-Cs134	③-Cs137
decay rate		219	1705	219	1705	219	1705
count(sample)	Gross	4281	25625	4297	25452	4499	25665
weight(sample)	g	7.831	7.831	7.831	7.831	7.831	7.831
count(STD)	Gross	41	142	41	142	55	132
weight(STD)	g	0.558	0.558	0.558	0.558	0.558	0.558
count(Blank)	Gross	40	74	40	74	35	53
radiation	Bq/kg	66180	45650	66430	45341	3483	39387
total	Bq/kg	111830		111771		42870	

UTNREATED SOIL #2							
Cs		①-Cs134	①-Cs137	②-Cs134	②-Cs137	③-Cs134	③-Cs137
decay rate		219	1705	219	1705	219	1705
count(sample)	Gross	2590	15060	2622	15026	2654	14867
weight(sample)	g	4.733	4.733	4.733	4.733	4.733	4.733
count(STD)	Gross	34	149	34	149	34	149
weight(STD)	g	0.558	0.558	0.558	0.558	0.558	0.558
count(Blank)	Gross	41	86	41	86	41	86
radiation	Bq/kg	(9402)	47777	(9520)	47669	(9638)	47161
total	Bq/kg	47777		47669		47161	

UTNREATED SOIL #3		①-Cs134	①-Cs137	②-Cs134	②-Cs137	③-Cs134	③-Cs137
Cs							
decay rate		220	1705	220	1705	220	1705
count(sample)	Gross	2958	17904	3026	17197	3121	17900
weight(sample)	g	4.753	4.753	4.753	4.753	4.753	4.753
count(STD)	Gross	33	122	33	122	33	122
weight(STD)	g	0.558	0.558	0.558	0.558	0.558	0.558
count(Blank)	Gross	29	72	29	72	29	72
radiation	Bq/kg	18912	71387	19352	68557	19965	71371
total	Bq/kg	90300		87908		91336	

UTNREATED SOIL #4		①-Cs134	①-Cs137	②-Cs134	②-Cs137	③-Cs134	③-Cs137
Cs							
decay rate		225	1708	225	1708	225	1708
count(sample)	Gross	3684	21269	3751	21277	3781	21490
weight(sample)	g	5.914	5.914	5.914	5.914	5.914	5.914
count(STD)	Gross	51	123	51	123	51	123
weight(STD)	g	0.558	0.558	0.558	0.558	0.558	0.558
count(Blank)	Gross	37	65	37	65	37	65
radiation	Bq/kg	5530	58916	5632	58938	5677	59530
total	Bq/kg	64446		64570		65207	

Southwest Research Institute Analytical Report

Analytical Report

Total Cesium Determination

Prepared by
Jackie Ranger

Prepared for
Kennesaw State University
SwRI Project Number 23231.06.009
SwRI Task Order Number 180212-5

INTRODUCTION

Eight soil samples and one water sample were received at SwRI on February 8, 2018 for total cesium determination and XRD analysis. The samples were logged into SwRI's Laboratory Information Management System (LIMS) under Sample Receipt Record (SRR) #61144 and were assigned to task order #180212-5. Table 1 contains the sample information.

Table 1 Sample Information

SwRI System ID	Customer Sample ID
627221	DI H2O
627222	Treated #01
627223	Treated #02
627224	Treated #03
627225	Treated #04
627226	Pretreatment #01
627227	Pretreatment #02
627228	Pretreatment #03
627229	Pretreatment #04

EXPERIMENTAL

Two analytical techniques were utilized for this project. They were X-ray Diffraction (XRD) and Inductively Coupled Plasma – Mass Spectrometry (ICP-MS).

XRD

Samples Pretreatment #01 (SwRI System ID 627226) and Treated #01 (SwRI System ID 627222) were analyzed via X-ray Diffraction (XRD) using a random mount orientation. The instrument utilized was a Siemens Kristalloflex 805 with a D500 Goniometer. The XRD spectra obtained with d-spacing scale, including the XRD library pattern matches, are provided as Figures 1 and 2. Optical photos of the two samples are included in Figures 3 and 4.

ICP-MS

Aliquots of the soil samples (approximately 100 milligrams) and water sample (approximately 2.5 grams) were readied for ICP-MS analysis via an open vessel, mixed acid digestion using nitric, perchloric, hydrofluoric, and hydrochloric acids. The resulting digestates for the eight soil samples contained residues. The residues were separated, dried, and fused with a lithium metaborate/tetraborate mixture. Both preparations were analyzed for cesium via Inductively Coupled Plasma – Mass Spectrometry (ICP-MS), using SW-846 Method 6020 as a guide. The instrument utilized was a Perkin Elmer DRCII ICP-MS.

For the soil samples, the reported cesium results are the sums of the cesium concentrations from the two preparation batches, with the exception of Sample ID Pretreatment #03. Cesium was not detected in the residue fusion preparation above its reporting limit for that sample.

All instrument quality control criteria were evaluated. The percent recoveries for cesium were within 90-110% for the initial and continuing calibration verifications (ICV/CCV). Cesium was not detected above SwRI's reporting limit in the initial and continuing calibration blanks (ICB/CCB). The low level, check standard recoveries were within 80-120% for cesium. The percent recoveries for the ICSAB interference check samples were within 80-120%. The limits were met for the ICSA interference check samples. The ICSA limits are the ICSA true value ± 2 times the reporting limit. The rhodium internal standard recoveries were within 80-120% for the ICV/CCV/ICB/CCBs, and within 30-120% for the reported samples.

Preparation blanks (or negative controls) were generated during both sample preparation batches. Lab ID PB18B22KE1 was for the initial mixed acid digestion. Lab ID PB18B27KE1 was for the residue fusion preparation. Cesium was not detected in either preparation blank above the associated reporting limits.

Laboratory control samples (or positive controls) were also prepared with the samples. NIST SRM 278 Obsidian Rock was utilized as the solid laboratory control sample for both preparation batches. The sample IDs are LCS18B22KE2 (for the initial mixed acid digestion) and LCS18B27KE1 (for the residue fusion preparation). The cesium recoveries were 92.5% and 54.4%, respectively. It should be noted that the NIST provided content value for cesium is not certified and is included for information only. An aqueous laboratory control sample (ID: LCS18B22KE1) was prepared during the initial mixed acid digestion. The cesium recovery was 101%.

Sample ID Treated #02 was prepared in duplicate. The relative percent difference (RPD) was less than 20% at 3.6%. The matrix spike (MS) analysis was performed on Sample ID Treated #04. The cesium recovery was within 75-125% at 79.9%.
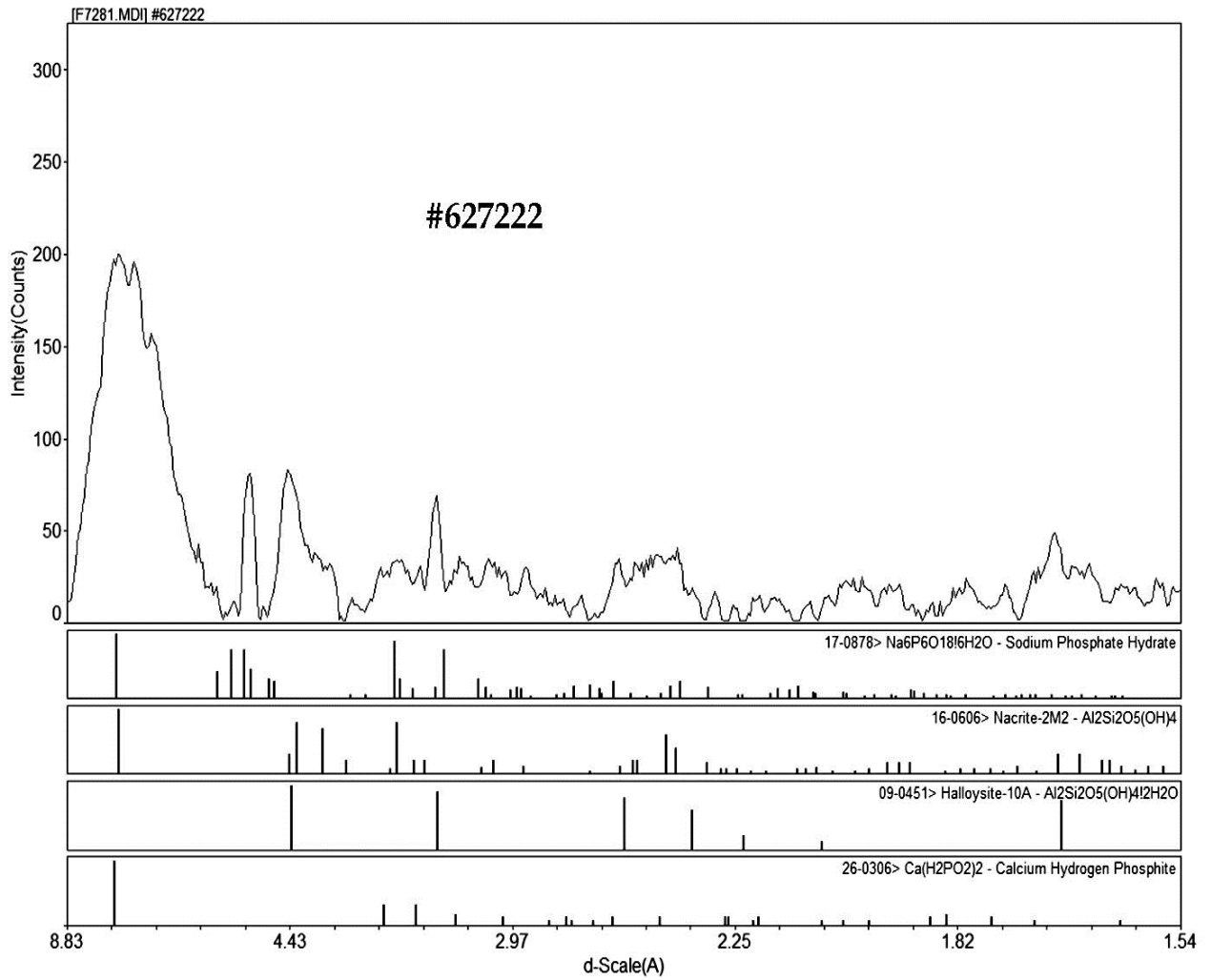
All cesium results are provided in Appendix A.
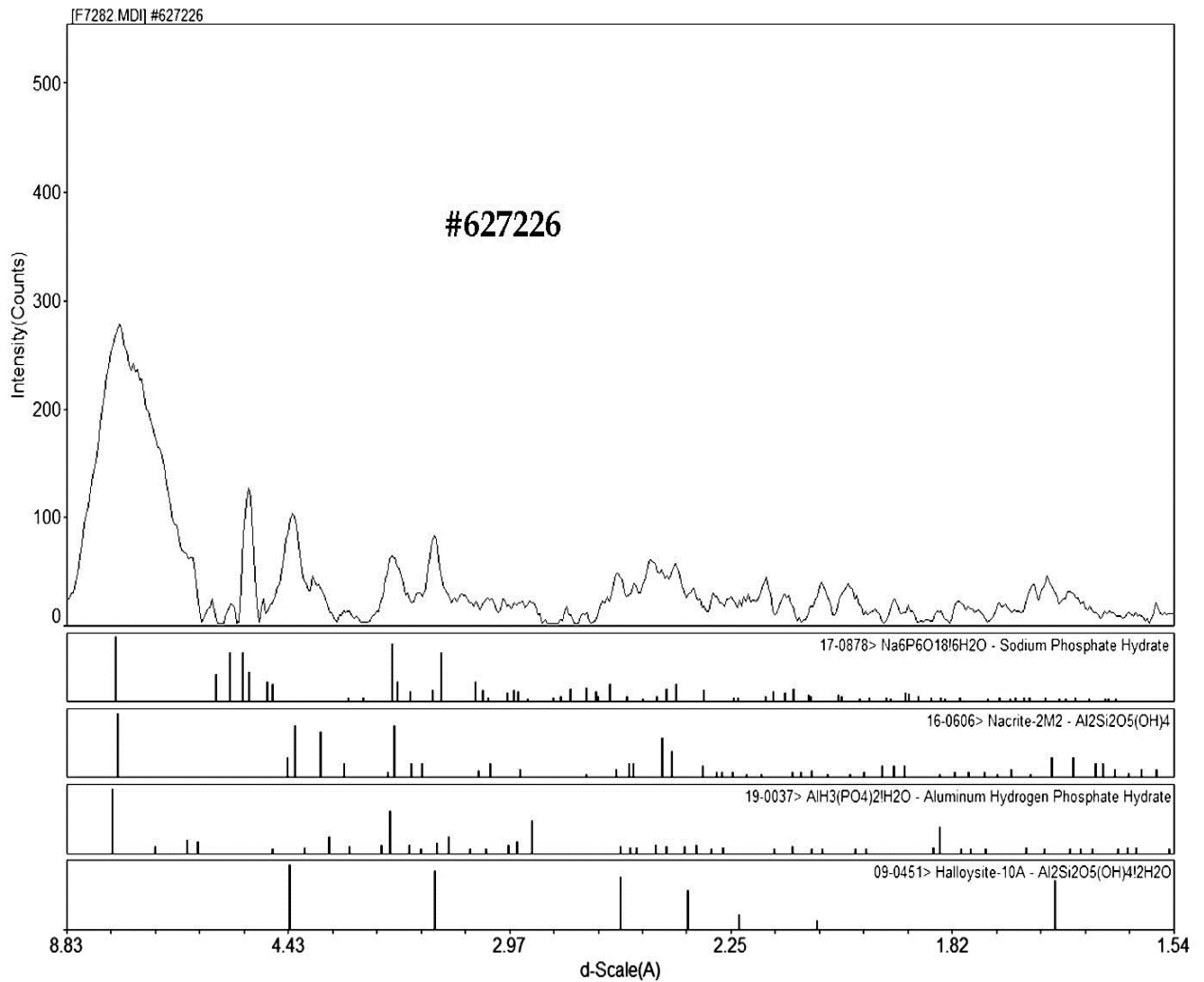
Figure 1. XRD of Sample Pretreatment #01, SwRI System ID 627226

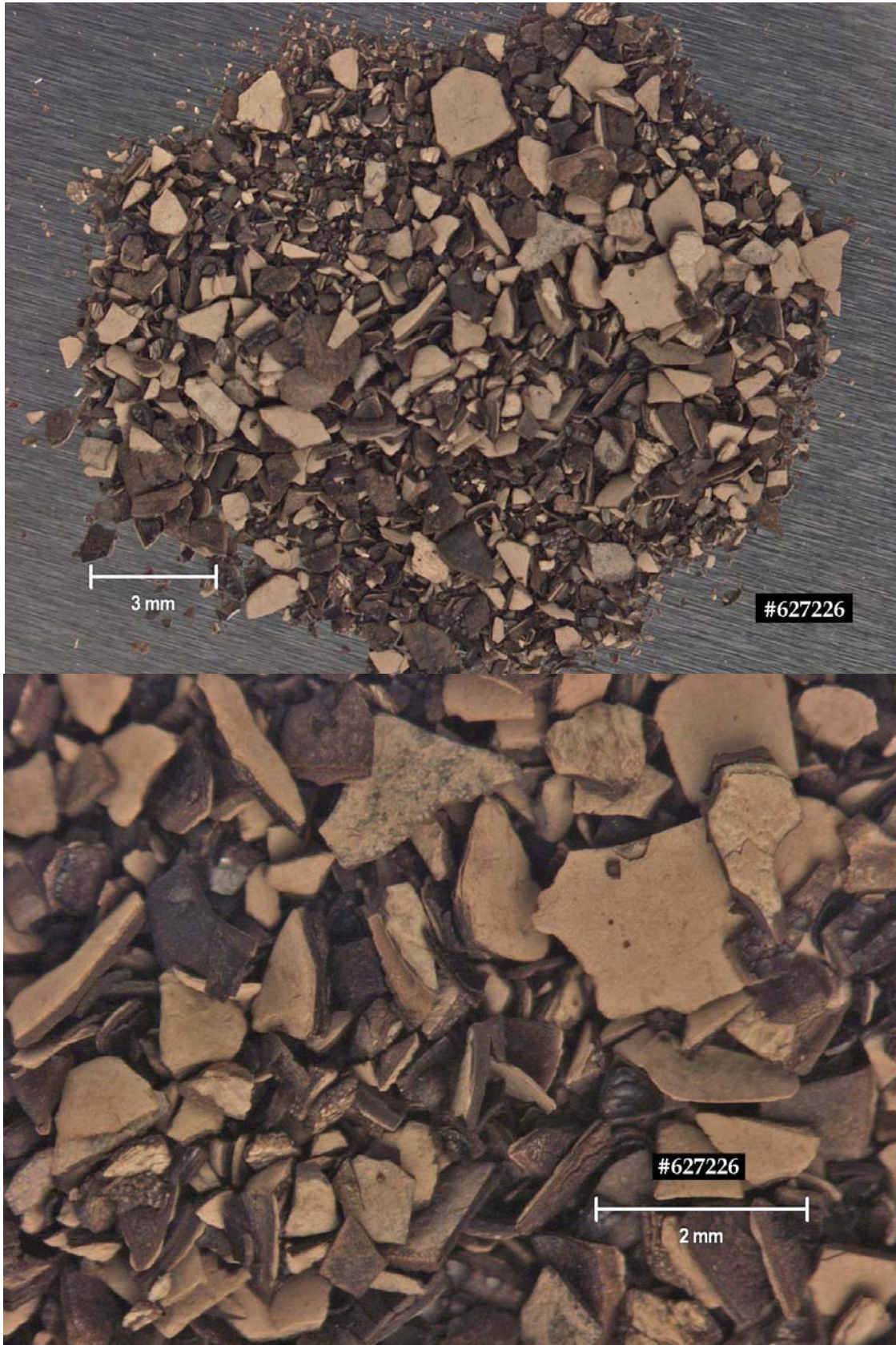Figure 2. XRD of Sample Treated #01, SwRI System ID 627222

Figure 1. Photos of Sample Pretreatment #01

Figure 1. Photos of Sample Treated #01

Appendix A
Cesium Results

SOUTHWEST RESEARCH INSTITUTE
SAMPLE ANALYSIS DATA SHEET

Lab Name: Southwest Research Institute

Lab Code: SwRI

Matrix: Soil

SRR #: 61144

Task Order #: 180212-5

Client: Kennesaw State University

Project No.: 23231.06.009

Date Received: 02/08/2018

PO #: 1008060

Sample ID	Lab System ID	**Cesium Results**	Q	Reporting Limit	Units	Date Analyzed
Prep Blank 1	pb18b22ke1	0.0150	U	0.0150	mg/kg	03/01/18
Prep Blank 2	pb18b27ke1	0.250	U	0.250	mg/kg	02/28/18
Lab Control	lcs18b22ke1	202		0.750	mg/kg	03/01/18
True Value	----	200		----	mg/kg	----
Recovery	----	101%		----	----	----
Lab Control 1 SRM278	lcs18b22ke2	5.09		0.267	mg/kg	02/28/18
True Value (Note 1)	----	5.50		----	mg/kg	----
Recovery	----	92.5%		----	----	----
Lab Control 2 SRM278	lcs18b27ke1	2.99		0.693	mg/kg	02/28/18
True Value (Note 1)	----	5.50		----	mg/kg	----
Recovery	----	54.4%		----	----	----
DI H2O	627221	0.000590	U	0.000590	mg/kg	03/01/18
Treated #01	627222	4.07		0.311	mg/kg	02/28/18
Treated #02	627223	3.09		0.317	mg/kg	02/28/18
Duplicate result	627223D	2.98		0.311	mg/kg	02/28/18
RPD	----	3.6%		----	----	----
Treated #03	627224	2.45		0.309	mg/kg	02/28/18
Treated #04	627225	2.96		0.312	mg/kg	02/28/18
Spike result	627225MS	154		0.308	mg/kg	02/28/18
Spike added	----	189		----	mg/kg	----
Recovery	----	79.9%		----	----	----
Pretreatment #01	627226	10.9		0.321	mg/kg	02/28/18
Pretreatment #02	627227	6.05		0.315	mg/kg	02/28/18
Pretreatment #03	627228	5.78		0.0723	mg/kg	02/28/18
Pretreatment #04	627229	6.46		0.311	mg/kg	02/28/18

Q - Data Qualifier. "U" in the qualifier (Q) column indicates undetected.

Note 1: The cesium result is provided on the Standard Reference Material 278 certificate, but it is not certified and included for information only.

www.manaraa.com